CHALMERS
UNIVERSITY OF TECHNOLOGY

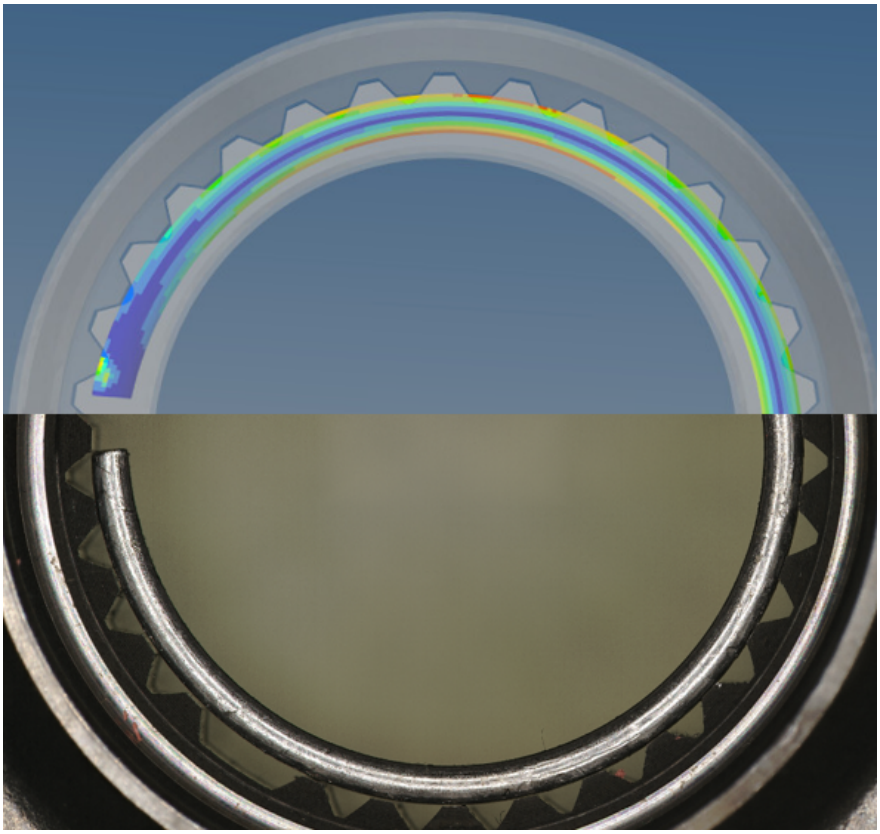

Snap Ring Joint Design for Transmissions at Volvo Cars

Master's Thesis in Production Engineering

Leo Anderson Naveda

Department of Industrial and Material Science

CHALMERS UNIVERSITY OF TECHNOLOGY
Gothenburg, Sweden 2021
www.chalmers.se

Project Report 2021:IMSX30

Design of a Snap Interface on Splined shafts

Improving the interface between a drive shaft, a differential gear and a snap ring to optimize assembly and disassembly forces

LEO ANDERSON NAVEDA

CHALMERS
UNIVERSITY OF TECHNOLOGY

Department of Industrial and Material Science
Division of Production Systems
Chalmers University of Technology
Gothenburg, Sweden 2021

Design of a Snap Interface on Splined shafts
Improving the interface between a drive shaft, a differential gear and a snap ring to optimize assembly and disassembly forces
Leo Anderson Naveda

Supervisor: Daniel Larsson, Volvo Car Corporation, Electric Diveline Department
Examiner: Magnus Evertsson, Industrial and Material Science

Master's Thesis 2021:IMSX30
Department of Industrial and Material Science
Division of Production Systems
Chalmers University of Technology
SE-412 96 Gothenburg
Telephone +46 73 145 4344

Cover: FEM simulation of the assembly of a snap ring on the top, snap ring sliding through a gear in reality on the bottom.

Printed by Chalmers Reproservice
Gothenburg, Sweden 2021

Design of a Snap Interface on Splined shafts
Improving the interface between a drive shaft, a differential gear and a snap ring to optimize assembly and disassembly forces
Leo Anderson Naveda
Department of Industrial and Material Sciences
Division of Production Systems
Chalmers University of Technology

Abstract

While the Volvo Car Corporation's mission is to develop cars which will fulfill the customers expectations, the ergonomics of the technicians and mechanics is also taken into account. This study was carried out to optimize the design of the interface between the front left driveshaft and the gearbox differential to make it possible to assembly and disassemble with a snap fit. The study considers previous analytical studies in split rings as well as mathematical models in order to try to comprehend the forces acting on it during assembly and disassembly. Some parameters were tested in the workshop and later on in the Universal Testing Machine to obtain data from several different experiments. After having understood the model and having data to compare, a Finite Element Method was developed to be able to test further parameters. Once the model reassembled the tests previously carried out, a Design of Experiments was carried out using a response surface tool. Using this tool, the parameters which affect more the assembly and disassembly forces were identified. Results from the modeling don't quite resemble the reality as the interface is very sensitive for contact and geometric imperfections but serve as a base to understand the most influential parameters. Finally, a new design was proposed based on all the previous experiments. Further recommendations for this topic are also given for alternative designs and what to avoid when designing a new ring.

Keywords: Snap ring; disassembly force; splined interface; driveshaft; snap design; ANSA; Contact modelling; Volvo Car Corporation; Differential gear; Retaining ring
.

Acknowledgements

This thesis was carried out in the All Wheel Drive department at VCC under the supervision of Daniel Larsson and Mats Strandberg. The thesis was carried out at Torslanda in Gothenburg during the Spring of 2020. This is the final report for the master thesis in the Production Engineering master program at Chalmers University of Technology.

I would like to extend my gratitude with the AWD group for taking me in and being supportive. Special thanks to everyone in SVS for their collaboration. To Morgan Karlsson and Thobias Hall in the propulsion workshop for the training in disassembling of gearboxes. To Raoul for guiding me in the simulation process, but even more thankful with Jing and Sarat who saved countless hours in troubleshooting the softwares used by the CAE department. To Ulf Johansson for the support and to Tony Sporrong for all the help with the measurements.

At Chalmers, to Håkan Johansson who acted as a supervisor and to Jim Brouzoulis who helped with some simulations. To Janne and Reine who helped me manufacture parts and lent tools. Special thanks to professor Antonio Strozzi from the university of Modena and especially to Enrico Bertocchi who discussed one of his papers and helped me write this report even under very difficult circumstances.

Pero mas importante, a mis padres, por todo.

Leo Anderson Naveda, Gothenburg, May 2020

Contents

List of Figures

List of Tables

Nomenclature

Δ	Radial Interference
α	Angular Width of the Ring
α_w	Angle of the Wedge Tool
β	Contact Angular Width
μ	Static Friction Coefficient
σ_{UTS}	Tensile Strength
σ_y	Yield Strength
θ	Ramp Angle
ζ	Self Locking Angle
c	Vertical Distance from the Neutral Axis
D	Distance traveled after impact
d	Deformation
E	Total Energy
E	Youngs Modulus
F	Axial Force
F_{impact}	Impact Force
F_{ins}	Axial Insertion Force
g	Gravitational Acceleration
h	Height
I	Moment of Inertia of a Cross Section
ID	Inner Diameter
KE	Kinetik Energy
M	Bending Moment
m	Mass
N	Normal Force
OD	Outer Diameter
P	Load Acting on the Ring
R	Radial Force
$R_{housing}$	Inner Radius of the Housing
R_i	Inner Radius of the Ring
r_m	Radius at the Neutral Axis of the Ring
R_o	Outer Radius of the Ring
R_p	Surface Roughness Maximum Peak Height
R_{ring}	Outer Radius of the Ring
R_z	Surface Roughness Mean Depth
Ra_{max}	Surface Roughness Distance Between Maximum Peak and Lowest Valley

SF	Safety Factor
t	Radial Thickness
U	Strain Energy
V	Volume
w	Axial Thickness

1
Introduction

This chapter gives an introduction of what a Snap Ring connection is, its main function and application at Volvo Car Corporation (VCC).

1.1 Background

The front driveshafts on a car transfer torque from the differential in the gearbox so that front wheels can turn producing grip to make the vehicle move. A differential is placed in between the left and right front shafts so that wheels can turn with equal torque at different speeds to improve the vehicle dynamics when turning.

The design of the driveshafts is part of the responsibilities at the Transmission department in Volvo cars. These components are designed so that they can be used for the car's full lifetime without having any severe damages which makes the removal of these parts unusual.

It is important during the design to make sure that parts are easy to repair or change to fulfil the aftermarket and give the customer the best experience. In a market of constantly changing requirements, VCC has opted to give customers not only low costs and high quality but also a personal and continuous service to add an extra added value to the brand. This means that spare parts have to be available even after 15 years and that the disassembly tools needed for a mechanic are to be available worldwide. This is one of the measures taken by VCC in order to move towards a circular economy with durable and repairable products.

In the year 2019 VCC sold an impressive 705,452 cars worldwide [1]. With 7 manufacturing plants, this still means that some plants have to run day and night to be able to cope with market demands.

1.2 Current Interface

In order to keep on building knowledge within VCC, a study is to be conducted on the ideal interface for the spline connection between the shaft and the differential gear. This shall serve as a background when giving specifications to suppliers instead of adapting to what suppliers have to offer.

The driveshafts are comprised of a solid steel shaft with a constant velocity joint on each end. The joints have splined ends to transfer torque through the differential gear to the wheel. The splined end on the shaft which leads to the gear has a groove where a mechanical component called snap ring sits in. On the differential gear, one end is closed with a lid to prevent the oil from the differential to leak out. On the other end, there is a female spline matching that of the driveshaft, this spline includes a bore which aligns to the groove of the shaft.

The function of the snap ring is to stop the driveshaft from sliding axially after being assembled. This snap ring is inserted axially to the shafts groove. When sliding the splined end of the shaft into the gear, the snap ring compresses to the same diameter of the female (gear) splines teeth until the groove and the bore match. At this point, the snap ring is free to expand as big as the bore diameter, this prevents the shaft from sliding out. Figure 1.1 shows a cross section of the interface along its axis and Figure 1.2 shows a close up on the interface between the three bodies.

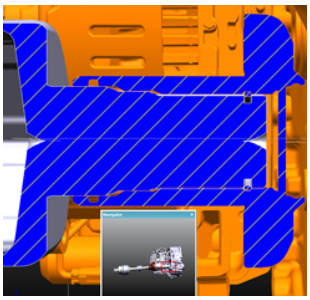

Figure 1.1: Cross section of the current interface.

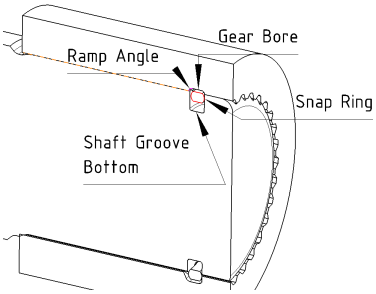

Figure 1.2: Close up of the interface with a simplified gear.

The bore includes a small ramp angles which allows the snap ring to contract while sliding out instead of being completely blocked as it is in the groove of the shaft. The terms explained in the picture will be used extensively throughout the study.

1.3 Problem Description

Currently, there is a high variation in the assembly and disassembly forces and the cause of this variation is unknown. In order to keep on building knowledge within the company, the current interface is investigated. The assembly forces of the shaft into the gearbox, as well as the disassembly forces, have to be within Volvo's internal specifications. Since there is no standard method available for the type of joint connections, a new interface had to developed in order to secure both assembly and disassembly for production and aftermarket.

1.4 Objectives

The objective of this study is to analyse the parameters on the interface to understand how they affect the assembly and disassembly of the shaft to obtain the best

possible design for the interface. Additionally it is aimed to find out what is causing the variation in disassembly forces. Currently, the operators assemble the shafts into the gearboxes quickly in order to keep up with the takt. The proposed interface has to also consider an easy assembly to keep the flow in the production and do not affect the ergonomics of the operators. The new design of the whole interface shall be assembled and disassembled within Volvo's internal specifications by pulling the shaft in the axial direction.

"Disassembly is a systematic approach that allows removing a component or a part, or a group of parts or a sub assembly from a product... during a disassembly the following factors can induce uncertainty: defective parts, disassembly damage" [2]. This means that the interface should not be damaged after every disassembly as it could cause the following disassembly to increase in difficulty or functionality to be affected. Achieving this will require designing a robust method and or tool which is to be distributed to all service centers world wide. The study will investigate what the root cause of the problem is and investigate as many parameters in the interface as possible.

1.5 Scope & Limitations

Additional to the time constraint of 5 months, other resources such as computing time, physical parts for testing and testing equipment also limit the scope of this study. Most of the research is to take place at the VCC facilities where assistance from engineers and mechanics is easy to obtain.

Although it is known that the ergonomics of the assembly or disassembly of the shaft is maybe an issue, this will not be researched into further. Disassembly tools and method will be tested and compared but no thorough research will be made to decide which is the recommended one as it involves researching possible damages in other parts of the gearbox. Additionally, designing a disassembly method requires knowledge on what is feasible to implement in all the VCC repair centres. Some parameters on shafts and gears are set as design guidelines within VCC and will be followed as they are, meaning that they will not be modified. The threshold for the push in and pull out forces are also outside of the scope of this study as they are also part of the design guidelines.

2

Theory

This section summarizes the theoretical knowledge gathered in an early stage of the project and is needed to understand certain sections of the report.

2.1 Snap Rings

Snap rings are machine components designed to act as a physical stop in the axial direction for rotating components such as shafts. Also often and mistakenly called, circlips or retaining rings, there is a vast variety of them in the market, designed for very specific purposes as well as standardized ones. Snap rings differ from retaining rings and circlips in the fact that snap rings are designed to take a certain axial load but to deform when the load is higher to allow the disassembly of the system. Snap rings therefore are intended to be removed and don't require a special tool to be dismounted, besides from the one needed to apply an axial force into the ring. These machine components are commonly classified as internal and external rings, depending on if they are encompassed on its extrados (outer perimeter) or intrados (inner perimeter). They can also be divided in axial or radial rings, depending if they are installed axially or radially into the shaft.

Snap rings are usually manufactured from large steel wires and rolled through shaping mills until the desired profile is achieved. The wire is then coiled into a certain radius and sheared off to form the final part. Bigger snap rings and circlips can also be cut from a piece of sheet metal. This limits the profile on the ring but also allows more complicated shapes and a variable cross section to obtain a more uniform circular deformation when compressed. The distance between the open ends can have different configuration in distance and angles at which the ring is cut. Each configuration is designed for a certain application which often considers serviceability and may require a special installation tool. Some rings have a beveled profile or a free helix to compensate for stacking tolerances according to [3].

Common materials are hard drawn, oil tempered and stainless steels. Rings can also be coated with a protective layer against corrosion, the most common ones are phosphating or zinc plating. Some rings are then stress relieved for optimal performance [3]. General dimensions for a snap ring include outer diameter (OD), Inner diameter (ID), radial thickness (t), axial thickness (w), distance between open ends (Gap), angular width (α) and profile shape. All of these measurements are affected by the manufacturing tolerances.

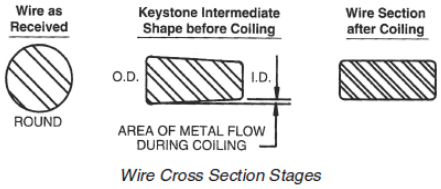

Figure 2.1: Shaping of the cross section in wire extrusion [3]

2.2 Manufacturers Guidelines

In order to choose the best ring, there are many design guidelines provided from the manufacturers and are often different from each other. Some manufacturers offer comprehensive guidelines, mechanical design formulas and recommendations which can be helpful when designing a snap ring interface. Groove design, shaft, design, max stress, stress during assembly are some of the formulas found in the handbooks [3], [4] and [5]. All the design guidelines found are focused on retaining rings which are similar to snap rings but differ in the aspect that these are designed to hold as much thrust load as possible. Since the handbooks are specifically for retaining rings, the design guidelines will not be analyzed thoroughly but considered for the snap ring interface.

When external rings are used, a loosening speed has to be acquainted for as the ring will fly out at a certain rotational speed due the centrifugal forces. This will be disregarded as high speeds will only cause the inner ring sit more tightly in the bore of the gear.

According to [3], [4] and [5] some of the important factors in the interface according to manufacturer's guidelines are shown in Figure 2.2. These are some examples of the parameters on the interface and the objective in this study is to test them and see how they influence the axial forces needed to mount and dismount the shaft into the gear.

2.3 Ring Geometries

Due to the countless number of different applications for these mechanical components, there is almost as many unique ring designs. They vary on the ring geometry, profile or cross section and gap. Each geometry and profile will have a different cross section and area moment of inertia and will affect how the ring deforms given the loads applied to it. The geometries will also affect the contact between the interface. As mentioned previously, the manufacturing of the ring will also limit the shape and cross section on the ring. This research will be done upon standard geometries and shapes which are already in production as coming up with an entirely new design would imply very high costs and possibly take longer time.

Housing	Shaft	Ring
Material properties: E, σ_y, σ_{UTS}, hardness, Poisson's Ratio	**Material properties**: E, σ_y, σ_{UTS}, hardness, Poisson's Ratio	**Material properties**: E, σ_y, σ_{UTS}, hardness, Poisson's Ratio
Groove depth: ≅ 0,99 Rings OD to obtain an interference fit. Not bigger than 4mm in 30mm rings DIN 161 section 6.	**Groove depth**: ≅ ⅓ of the rings radius. Should allow rings compression.	**Shape**: Axial shape
Bore width: Does not affect the load carrying capabilities.	**Groove width**: = 1.143 * Rings thickness (Smalleys) Desired to be minimum to remove axial play while considering stackable tolerances.	**Maximum stress**: During assembly< 100 σ_y to prevent plastic deformation.
Ramp angle: Allows the ring to deform and exit the bore.	**Groove tip radii**: Should be minimum to transmit load axially during assembly & disassembly	**Surface roughness**: influences the friction coefficient and can act as a physical stop.
Surface roughness: Influences the friction coefficient and can act as a physical stop.	**Shoulder width**: Affects the thrust load capabilities. It is desired that the shaft does not shear even in extreme cases.	**Geometrical properties**: OD, ID, axial width, cross section shape.
	Spline: Pitch diameter, number of splines.	**Gap distance**: Distance in between the open ends.

Figure 2.2: Table with some of the identified parameters in the interface and recommendation from design guidelines

2.4 Analytical Study

Split rings are bent beams with an angular width of maximum 2π and extensive studies have been written about them. Many of such studies were performed in split ring applications for pistons but are applicable to the researched snap ring. From Castigliano's theorem, the deflection of a beam can be calculated by derivating the strain deformation with respect to the force acting at a certain point as seen in (2.3). Since the loads required to compress a ring are mostly bending loads and the cross section of the ring is constant, the strain energy for half a ring can be calculated as follows.

$$U = \int \frac{2E}{\sigma^2} dV \tag{2.1}$$

Even though there are only bending stresses acting on the ring, they are not constant and therefore an integral is used to calculate the bending moments all along the ring.

$$U = \int_0^{2\pi} \frac{M^2}{2EI} d\alpha \tag{2.2}$$

Lastly, the deformation at a certain point, in the direction of a force applied can be calculated.

$$d = \frac{\partial U}{\partial F} \tag{2.3}$$

Another useful equation used to calculate the moments on a curved beam when being flexed into a smaller or larger radii is the following taken from [6].

$$\frac{1}{R_{housing}} - \frac{1}{R_{ring}} = \frac{M}{EI} \tag{2.4}$$

The bending moment can then be used to calculate the bending stresses on the beam or ring.

$$\sigma_{bending} = \frac{Mc}{I} \tag{2.5}$$

Where c is the vertical distance to the neutral axis.

Several studies have been performed on split rings. [7] Treats the rings as frictionless and uses a purely elastic theory in the study, considering the rings as "thin rings". "When Ro/Ri is smaller than 1.1 the ring is considered thin" [7]. His studies have also proved that axial and shear stresses on thin rings can be disregarded when sliding the ring into a cylindrical housing.

Snap rings are inserted with an interference fit and therefore have to deform in order to fit the housing. Figure 2.3 shows how this deformation occurs and divides the ring in section A-B and B-C. Where A-B is the contact width, B-C is the separation angular width where there is a gap between ring and housing. These points are further on referred to in this thesis. "The angular extent of the contact will be independent of the rings absolute dimensions but it will depend on the aspect ratio between the ring outer and inner radii ..." [8]. The study reveals that the contact forces act at about one third of the periphery between A-B and on the open ends at C, forces are punctual. Same result is reported by [6].

From [7], the contacting surface of the ring often undergoes Hertzian-type deformations, which are relatively small and also disregarded in his study. From [8] it was learned that the contact forces increase linearly with the interference between the rings extrados and the housings ID. In [8] it is proved that both the shear forces and the modification of the contact pressure are negligible compared to the flexural forces on thin rings. As the curved beam becomes thicker, the curvature effects increase and may not be disregarded if the rings are not considered as thin. In his study, [8] also assumes that the deformation is small compared to the rings OD (Outer Diameter).

Stresses within the ring attain high values in the vicinity of the ring extremities, where the ring housing contact width becomes very localized [8]. This can be better illustrated in 2.4.
Thin split rings can thereby be represented by Figure 2.5. Where F is a punctual centripetal force on the extremities of the ring, p is the contact pressure distributed

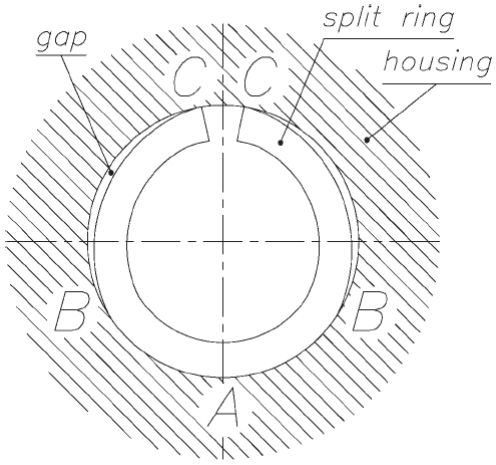

Figure 2.3: Snap ring deformed to fit a housing [8]

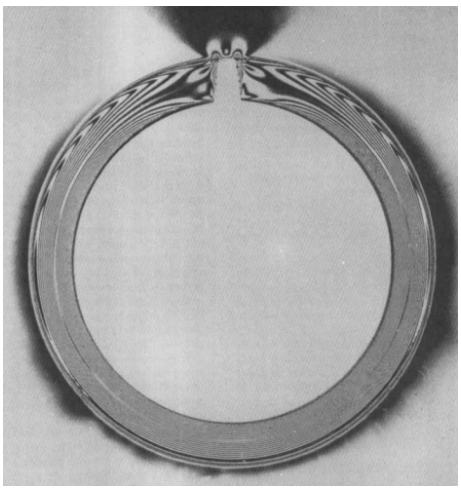

Figure 2.4: Stresses on a split ring compressed into a housing taken from [7]

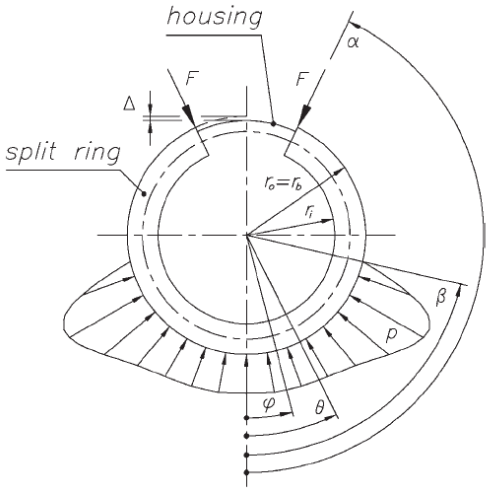

Figure 2.5: Forces acting on a split ring while deformed taken from [8]

along β. α is the rings angular width. Δ is the interference between the ring and the rigid housing. As stated previously, the separation section B-C from Figure 2.5 matches the angular width of β - α. Au contraire to the authors initial expectations and in continuation to studies from [7] and [8] proves that the separation zone B-C is independent of the angular width of the ring. The contact then diminishes as the angular width of the ring diminishes. The rings contact angular width β is independent of the Young modulus of the material and is linearly dependant of the interference with the housing.

The axial force needed to press fit the snap ring into its housing is calculated as follows and rests on several assumptions such as uniform contact along the rings extrados and a small deformation [8].

$$\frac{F_{ins}}{\mu} = \frac{E\Delta I}{{r_m}^3}[\tan(\frac{\alpha-\beta}{2}) + (\alpha-\beta) + \alpha)] \tag{2.6}$$

2.5 Snap Mechanisms

Snap components are components which can elastically deform in order to slide in or out of other geometries. Snap mechanisms are analytically analyzed in [9] and show that a critical parameter for the design of snap components is the angle or ramp angle. The engagement angle is the angle at which the contact between two components meet and slide, it is further referred to as ramp angle and can be found on the differential gear. Note that the differential gear has an entry and an exit ramp angle, used for assembly and disassembly respectively. A two way snap fit is when a component can be assembled and disassembled. In order for this to happen, the self locking angle ζ has to be avoided and can be found using the following equation.

$$\zeta = \arctan\left[\frac{1}{\mu}\right] \tag{2.7}$$

[9] Proposes three basic principles for snap component design:

1. Entry ramp angle = Exit ramp angle $\longrightarrow$ Force for assembly is equal to disassembly force
2. Entry ramp angle < Exit ramp angle $\longrightarrow$ Assembly force is smaller than the disassembly force
3. Entry ramp angle > Exit ramp angle $\longrightarrow$ Assembly force is greater than the disassembly force

This means that in order to be able to have a two way snap fit, the ramp angle on the gear has to be smaller than ζ. For the purposes of this study, the exit ramp angle on the bore of the gear has to be greater than the entry ramp angle in order to have lower assembly forces.

This can also be thought of that with a ramp angle close to 90°, it will act as a physical stop and normal forces will directly oppose the axial force to pull out. As the angle is decreased, the radial deformation becomes smaller over the axial displacement. The opposing force is transmitted more radially than axially and components are allowed to slide. When the angle tends to 0° there are no normal forces acting radially and the only component opposing the movement is dependent on the friction. This is illustrated in Figure 2.6.

2.6 Contact Mechanics & Friction

Surface roughness is a phenomena engineers have to cope with, and it is often related to higher manufacturing costs. For this reason, it is not possible to have all

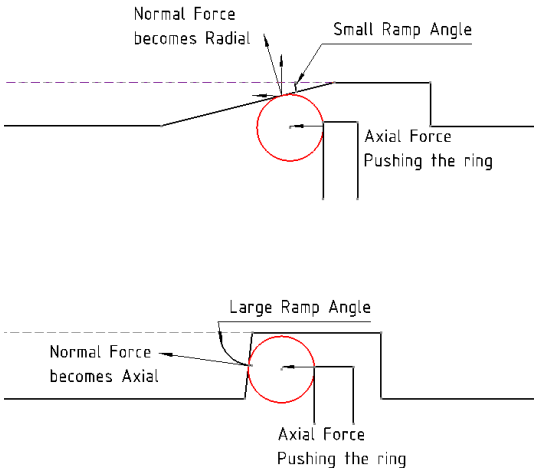

Figure 2.6: Axial force comparison with small and large ramp angles

surfaces smooth at the micro scale level and designs have to acquaint for the surface roughness presented after manufacturing.

The current surface roughness on the ramp angle of the gear is measured in R_z, stated by [10] as the mean roughness depth. Although there is no simple connection between surface roughness and friction coefficient many studies have been performed to try to explain this. According to [11], friction coefficient can increase up to 50% on milled surfaces compared to polished surfaces. This would suggest that a better surface roughness could help considerably in the disassembly if friction was the issue. Additionally, [12] shows that surface roughness parameter R_z has a big correlation to the static friction coefficient in many metals. While the most influential parameter is the mean slope of the roughness on the profile.

[13] Shows that sharp corners have big stress concentrations in interference fits. This supports the idea of having round edges on the contact surfaces. Additionally, sharp corners are more prompt to contact a surface defect and possibly get stuck.

2.7 Central Composite Design

Parameter studies are often performed to determine which factors on the system have the biggest impact in a certain output in a process. It is important to understand the independent and dependent variables in the system and often assumptions have to be made to reduce the number of variables. The Design of Experiments (DOE) can be used to plan which of the variables and values will be analyzed. The result is a design table with experiments to perform; its size increases exponentially with every factor to be investigated.

Response surface tools are used to analyze the behaviour of the variables in an

experiment without the need of testing all the values. ”The response surface is simply a regression equation that approximates model output using only the most sensitive model input parameters ” [14]. It is required to perform experiments with a low, medium and high value for each of the factors to create the regression equation. The response surface increases the number of tests to be performed in the DOE but in return, gives a better understanding of the impact of the factors within a range of values. There is a wide variety of scientific papers explaining these tools and therefore they will not be explained any deeper in this report.

3
Methods

This section describes the methods used in this thesis. A discussion of them is included further on.

3.1 Analytical Study on the Current Snap Ring

Based on the knowledge obtained from the theoretical study, the current rings will be analyzed to try to understand which loads act on the ring while assembling or disassembling the shaft. The objective is to try to estimate and predict axial forces for a certain ring using a mathematical model. A tolerance study was performed on the current interface and on the faulty parts to see if it was a quality or tolerance issue.

3.2 Field Study & Physical Testing

The main objective of this study is to find out what parameters causes the rings to get completely stuck. While, the rest of the methods aim to get a better understanding on how to design the optimal interface. Parts which shown high disassembly forces were kept for further analysis. The gearbox was installed into a test rig where different shafts and rings could be tested in both assembly and disassembly. The different assembly methods were tested and analyzed to to deliver a robust solution. Later on, different rings were tested according to suppliers recommendations and others were modified to identify which parameters would make the interface easier to disassemble. Finally, a benchmark was performed to see how other cars have the connection between shaft and differential gear.

3.3 Experimental Investigation

So far previous experiments and reports were based on subjective results. An assembly and disassembly rig was set up in a universal testing machine (UTM) in order to obtain numerical data to take decisions with. This test measures the pull out force for disassembly and push in force for assembly using an UTM. Data could be plotted in Matlab to obtain a displacement vs axial force curve, and identify the peak values and variation on different tests. The objective of this study was also to identify what causes the variations in axial forces between different samples, to

propose a new design. New designs could be later tested using an FEM model and correlate it with the data from the UTM to make sure results more significant.

3.4 Computational Model

As it is not possible to physically test some of the parameters identified from the analytical study without long lead times from suppliers, a computational model was developed based on [15]. This model is a Finite Element Method (FEM) simulation and was based on a static simulation of the assembly and disassembly of the system. A basic simulation of a half ring was performed using ANSYS. Later on a more complex assembly and disassembly simulation was made in ANSA using the Abaqus solver and reading the results in Meta post processor and Hyper viewer. Results from this model can be compared with the experimental study and model can be tuned until a close correlation is achieved. This model was then used to perform a DOE, modifying the parameters on the interface to obtain optimal values.

3.5 Parameter Study

Using the correlated computational model and based on [16] an experiment was designed. The aim was to identify the factors and interactions from the parameters of the interface which affect the assembly and disassembly forces the most. Performing the DOE using the computational model enables testing different materials, geometries and parameters which would take large lead times to obtain physical samples to test with. Data was processed using Minitab to obtain a response surface of the interaction between the factors and their impact on the response variable.

4

Results & Discussion

4.1 Analytical Study on the Current Snap Rings

In this section, the analytical study on the current parts based on the theory previously reported is explained. Experiments were developed based on previous results, for this reason this section acts as a guideline on how the research was carried out. Due to the large number of experiments performed in this section, some will be briefly discussed here.

4.1.1 Thin Rings

To make sure the papers reviewed in the theoretic study are applicable to the analyzed snap ring, later on referred to as current snap ring, the nominal dimensions were compared to see if they apply as a thin ring.

$$r_o = 16.45mm \rightarrow r_i = 15.625mm \rightarrow \frac{16.45}{15.625} = 1.05 < 1.1 \tag{4.1}$$

Therefore the ring object of this study may be considered as thin.

When an inner ring is installed, it suffers the highest stresses when being compressed to slide through the female spline and is partially relieved when reaching the bore. The contact will be then significantly reduced as predicted in the analytical study and shown in Figure 2.3. This can also be seen in Figure 4.1 where a ring was deformed into the gear and then scanned. The gap between the ring and the housing was measured and resulting in 0.262 mm.

It can also be noticed in the gear that two splines are missing in the shaft, reason for this is that the gear is completely sealed on the opposite end to prevent oil from leaking out from the differential. The missing splines allow air to go out during insertion. This provides a lower assembly force for operators and with it, better ergonomics. A recommendation is to increase the depth of the female splines, in this way, the air can escape during assembly and no torque is lost because of the missing splines. Further research should be conducted to make sure no stress concentrations are created.

From [7] it was learned that the angular width of separation is constant even when changing the angular width of the ring.

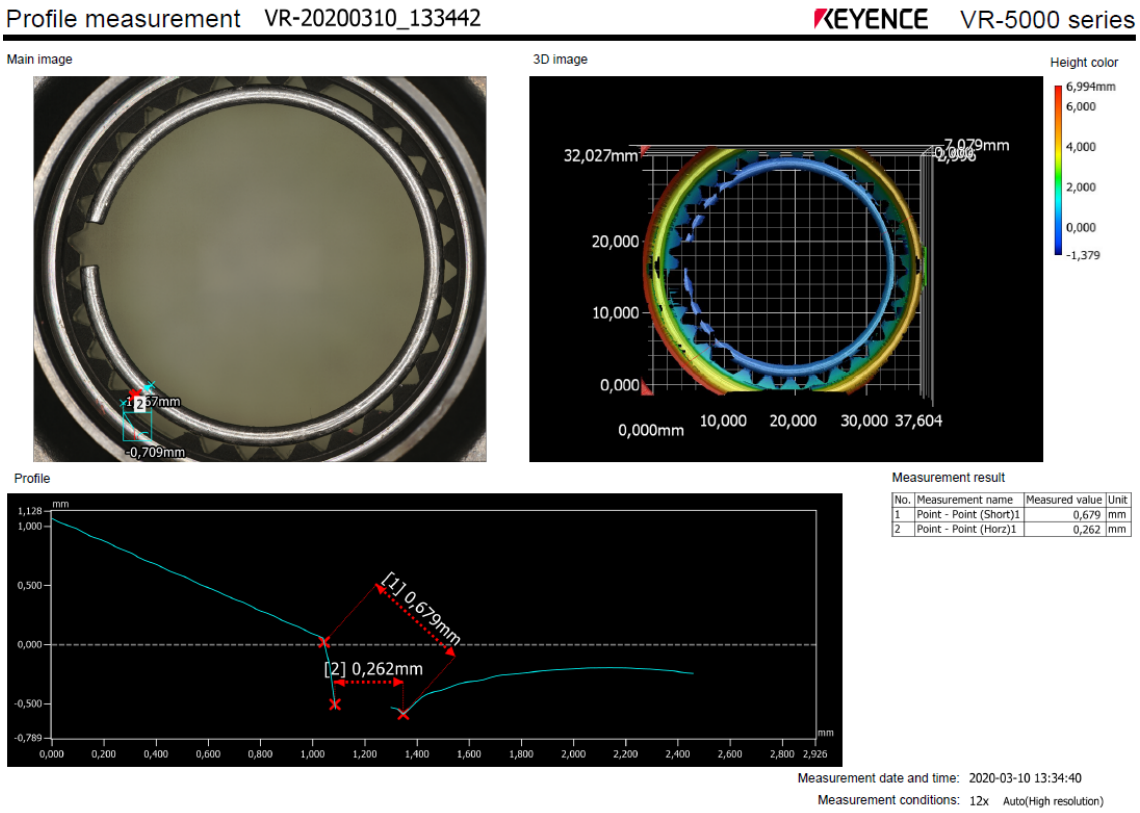

Figure 4.1: Measurement of a deformed ring inside the gear

$$(\cos(\alpha - \beta) + \frac{\alpha - \beta}{\sin(\alpha - \beta)}) = 2 \tag{4.2}$$

$$\alpha - \beta = 2.139Rad \rightarrow \alpha = 165 \rightarrow \beta = 0.740Rad = 42.34 \tag{4.3}$$

An enlargement of the contact in picture Figure 4.2, shows that the ring has contact only with 8 splines at a time (Region A-B) as shown in Figure 2.5. This means that the measured β is equal to about 46° on each half. Quite accurate to the angular contact width calculated by [7].

4.1.2 Forces Acting on the Ring

By making a cut of the cross section along the axis, the contact forces can be represented in a free body diagram in Figure 4.3. Considering that the upper contact has been lost and ignoring friction, the main forces acting on the ring are F (Pull out axial force), R (Radial force on the ring), N (Normal force acting perpendicular to the contact surface.

Using the snap theory from [9] it is known that the ramp angle $\theta = 64°$ has to be smaller than $1/\mu$. By reducing the ramp angle, the allowed friction coefficient is increased.

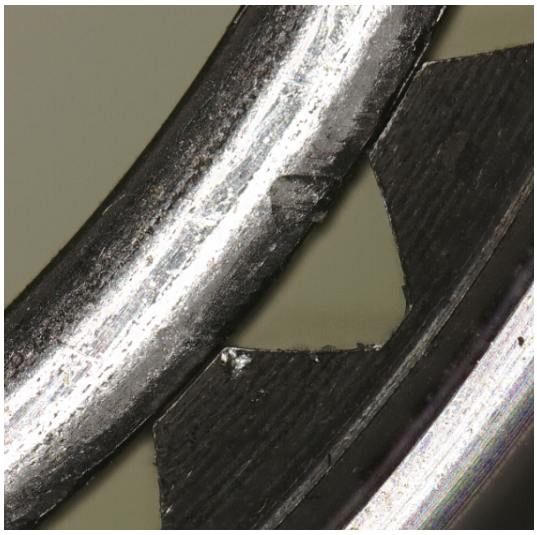

Figure 4.2: Separation on the ring and housing starts on the fourth spline

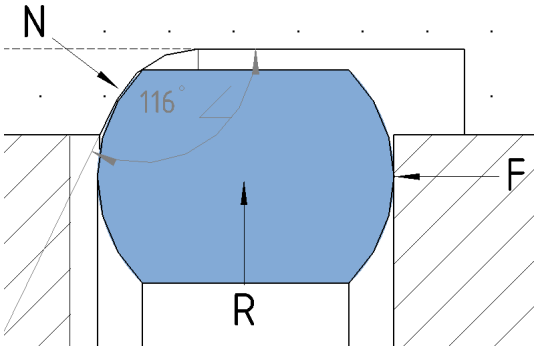

Figure 4.3: Free body diagram of the axial cross section on the sliding ring

The equations obtained from the free body diagram during slip conditions are the following.

$$R \leq N * \cos(\theta) \longrightarrow N = \frac{F}{\sin(\theta)} \rightarrow F = R * \frac{\sin(\theta)}{\cos(\theta)} \tag{4.4}$$

From (4.4) it can be noticed that the ramp angle relates the radial force to the axial force and that if friction is ignored, the ramp angle becomes a coefficient between both forces. Table 4.1 shows how much the force should be theoretically reduced at different ramp angles when ignoring friction.

Considering that the axial pull out forces may require the use of a hammer and that the ring is deformable with bare fingers there has to be a bigger factor in play. A ring was positioned vertically in a UTM and compressed until the open ends would touch each other due to the deformation. The vertical forces were measured and compared to the vertical displacement. To analyze the same experiment analytically, a symmetry assumption is used at A and the force is placed 90° from A according to the center of the ring. The open end will have a distance of half a gap to the x

axis. By using Castigliano's theorem and applying it to a thin curved beam similar to the ring, the following equation is obtained.

$$d = \frac{Pr_m^3}{EI} \tag{4.5}$$

Where d is the vertical deformation as measured in the UTM, P is the force applied on the ring which is also measured by the UTM and r_m is the radius at the normal axis on the ring. Experimental and theoretical forces are plotted showing very similar linearly increasing forces of only around 80 N to deform the ring 3 mm vertically. This explains why the ring is deformable with bare fingers as long as this is only in one direction.

In order to obtain the force needed to deform the ring radially, (2.6) is used. The resultant radial force per friction coefficient obtained was 338.82 N, assuming that the force is placed all around the extrados of the ring. Ignoring friction, the axial force needed to deform the ring under these assumptions would be of only 916.5 N. It is known however, that the forces are larger than what was estimated. In order to obtain a more accurate estimation, the equation would need to be modified as the assumptions made in [8] does not fit the case of this snap ring accurately. In reality, as explained in the theoretical study, there is a separation and force is not applied equally along the extrados.

The bending stresses on the ring at point A can be estimated using Castigliano's principle for bent beams (2.1). Considering a vertical load on C would cause the ring to open or close, the deformation on C would cause a bending stress at A which should be smaller than its yield strength to avoid a permanent deformation. The equation to obtain the bending moment at A is the following.

$$M = PR_m(1 + \cos(\alpha - \frac{\pi}{4})) \rightarrow P = \frac{dEI}{R_m^3(1 + \cos(\alpha - \frac{\pi}{4}))} \rightarrow M = \frac{dEI}{R_m^2} \tag{4.6}$$

Where d is the vertical deformation at the open tips.

$$\sigma_y \leqslant \left[\frac{Mc}{I}\right] SF \tag{4.7}$$

Since the scope of this study is not to find a valid mathematical model, and the model would increase in complexity when analyzed rings are not round, the analytical study

Table 4.1: Estimated axial force variation by decreasing ramp angle

Ramp Angle (°)	**tan (θ)**	**Force reduction compared to current ramp angle**	**Reduction to previous ramp angle**
64	2.05	0%	-
61	1.8	12%	3.74%
57	1.6	21.95%	3.12%
54	1.42	30.34%	2.65%

was terminated. Although this section did not successfully estimate the disassembly forces, some important parameters where identified and are analyzed further in this report.

4.1.3 Material Properties

The material properties of the gear and shaft will also play a big role as it is not intended to damage any of the components. These components are induction hardened to a superior hardness than the hardness of the snap ring. The current snap ring is shaped from a hot rolled steel in accordance to C72D and heat treated at 400° C to increase the base material hardness. The ring is then polished in a rotating barrel with abrasive particles to remove any burrs and improve the surface finish. Finally, the ring is coated with oil to improve its corrosion properties.

Obtained from the supplier, the hardness of the heat treated ring has an average of 46 HRC and a tensile strength (σ_{UTS}) of 1,620 MPa while the yield strength (σ_y) lies around 1,420 MPa. To verify the tensile strength, a tensile test was done by straightening the ring wire and testing it in the UTM as shown in Figure 4.4. The tests showed a maximum of 1,700 MPa.

Figure 4.4: Tensile test on an unbent snap ring

4.1.4 Surface Roughness

One hypothesis of the root cause was that the surface roughness would prevent the relative sharp edges of the ring to get stuck and prevent sliding. Reason being because of the machined surface at the ramp angle showed visible burrs. One of the faulty gearboxes was tracked down and the supplier provided the measurements

from that the batch. These were inconclusive as there has not been any studies to determine what the tolerances on them should be. Surface roughness measurements in R_z from a batch with a gear believed to be faulty is presented below however, there was no measurement of the specific gear.

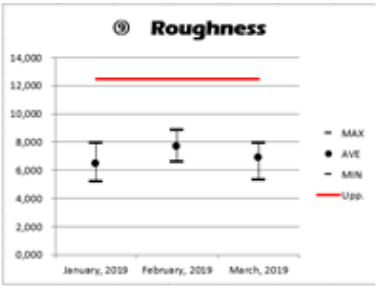

特性	MAX	MIN	AVE	Upp.	
Jan, 2019	7,890	5,170	6,436	12,5	
Feb, 2019	8,810	6,570	7,660	12,5	
Mar, 2019	7,920	5,280	6,856	12,5	

Figure 4.5: Surface roughness measurements and tolerances

Current specification is considered as "rough, low grade surface resulting from heavy cuts during machining" [10]. Note that some burs can be felt on some of the splines at the ramp, it is unknown how many of these splines the surface is measured at but it is very different from one spline to another. An optional parameter to be measured for surface roughness would be Ra_{max} which measures the distance between the highest peak and the lowest valley. This measurement is more sensitive to scratches and burrs whereas the average measurements can still be within tolerance even with consecutive burrs. R_p measures the maximum profile height of a peak which can also be used as a specification criteria. As understood from the theoretical study, the surface roughness can be responsible for increasing the friction coefficient, especially the R_z value [12].

4.1.5 Tolerance Study

Knowing how the rings are manufactured, it is understood that the parameters which will vary the most are the outer diameter and the gap distance. The cross section will vary less as it is rolled through tools, taking its shape. From the previous measurements done on the assembled ring, it can be seen that there is a separation between points B and C of the ring. This separation causes the open ends to get even closer together when the ring is fully deformed. The question which comes out is whether or not, the open ends could actually meet during the deformation of the ring. Considering tolerances, the ring with the biggest possible outer diameter is drawn in Catia. Tangent to point A, a circle with the gear inner diameter of the splines is drawn as seen in the following Figure 4.6. The undeformed ring is illustrated in grey while the gear female splines are illustrated in a transparent grey,

lastly, the deformed ring is the green body.

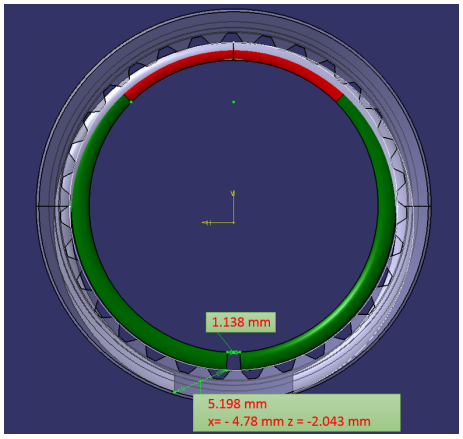

Figure 4.6: Deformation of an oversized ring

From the measurements, it was observed that there is contact between the ring extrados and the gear for about 45° on each half, illustrated with red line in Figure 4.6. From then, there is a maximum separation of about 0.262 mm on the ring and becomes smaller until the open ends of the ring have a punctual contact with the housing (point C). The perimeter should remain constant during the contraction of the ring. Meaning that the distance between the open tips of the ring is only 1.138 mm in the worse case. If a ring with a bigger outer diameter and a smaller gap is assembled, the open ends could touch, making this a mechanically locked system which would require shearing to remove. Additionally, the angle at which the ring is sheared, is not controlled for quality, this angle could also create a smaller gap between the open ends.

To prevent the open ends from touching during deformation, it is important that the gap is large enough. A simple formula was created for a reference to determine the minimum angular width of a ring.

$$R_{housing} * \pi + SF \geq \alpha * (\frac{ODmax}{2}) \tag{4.8}$$

$$\alpha = \sin^{-1}(\frac{gap}{ODmax}) + \frac{\pi}{4} \tag{4.9}$$

Where $R_{housing}$ is the minor radius of the gear, $ODmax$ is the largest possible outer diameter in the ring, SF is a safety factor, α is the angular width of the ring obtained from the gap between the open tips. Another interesting learning outcome from Figure 4.6 is that in that angular position, the contact will not be on the end of the open tips but in the adjacent splines. This can possibly also act as a mechanical locking as the open tips slightly stick out and close with a spline in between. If this is the case, the ring will have to be partially sheared, this theory is analyzed further on in the report.

4.2 Field Study

In this section, the results from the physical experiments performed at the workshop with different dismounting tools, modified rings, as well as the benchmarking are reported.

4.2.1 Dismounting Method

Different dismounting tools have been tried and depend on availability in different workshops. It is desired to design a dismounting tool which can work properly even when the required disassembly forces have a variation. The variation in dismounting forces has previously been tried to optimize using different rings from the supplier but there is still room for improvement. Current tolerances on the parts are set by the suppliers and it is unknown if these are optimal or could be responsible for the variation in axial forces.

Due to the limited space between the shafts joint and the gearbox and the overall packaging of the components, the disassembly tool design is limited. Figure 4.7 shows the first disassembly method. A bent piece of metal would be positioned between the joint and the gearbox and hammered on the other end to try to create an axial force on the shaft. It was believed that the tool would pivot on the upper end creating a contact only on the outer lower edge of the joint.

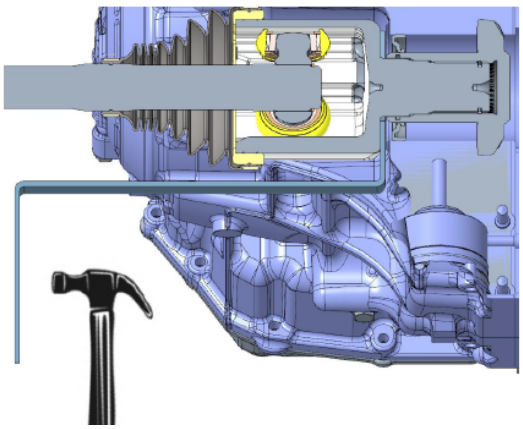

Figure 4.7: Dismounting method #1

4.2.2 Current Method

The current disassembly method consists of a wedge tool which is hammered perpendicularly to the axis of the shaft or using it as a lever, resulting in an axial force as shown in Figure 4.8. The axial force would push the shaft outwards, causing the snap ring to contract and then slide through the gear.

Figure 4.8: Shaft disassembly method using the wedge tool

The method works quite well in most cases even though it leaves some permanent damage in the gearbox housing as seen in Figure 4.9. There is possibly damage on the gear as well however not visible. In some fewer cases where the ring gets stuck, very strong hammer hits are needed to dismount the shaft, these may damage the above mentioned parts even more. Additionally, the wedge is positioned in a sensitive place on the gearbox housing where a conical support for a bearing is located internally. A new tool was developed to transfer an axial load with a hammer hit. The method was an improvement of the method #1 but had a more rigid structure to transfer the loads.

Figure 4.9: Marks on the shaft after disassembly

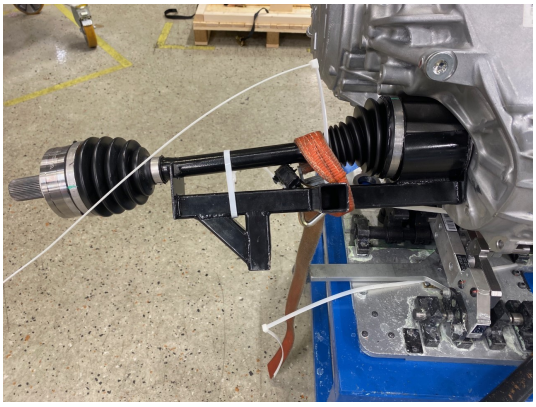

Figure 4.10: Dismounting method #3

Once a shaft got stuck, the method was tested at SVS as seen in Figure 4.10. The tool was hammered numerous times but the shaft stayed in place. The hypothesis generated was that as the impact was momentaneous so the ring could spring back into place. Deformation takes place during a split of second instead of slowly deforming in localized places. Once the shaft was successfully removed using the

wedge tool, the ring showed heavy indentation marks caused by the hammer hits. For this reason it is recommended to have a wedge tool with a small wedge angle (α_w) which will generate a small axial displacement compared to the vertical one. This solution also keeps a constant pressure on the ring so it would not snap back into place. This hypothesis would need to be investigated further.

4.2.2.1 Analysis of the Wedge Tool

In order to remove the ring from the gear's groove, it is necessary to exert an axial force in the opposite direction of the assembly. A free body diagram of how the shaft if disassembled is shown in Figure 4.11. It is noticeable that the angle of the wedge plays a big role as the load will be divided into axial and radial components. The radial component will cause a bending which is undesirable while the axial force is the component which will transmit the load to the snap ring through the shaft. To minimize the radial component, the angle α_w on the wedge can be minimized.

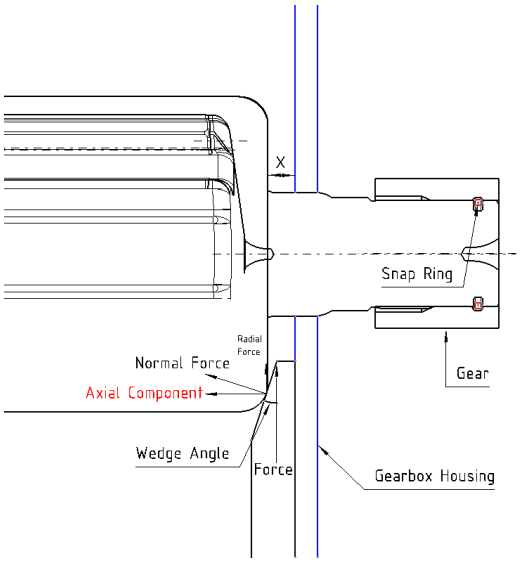

Figure 4.11: Free body diagram of the main forces during disassembly

There are some restrictions however, the vertical displacement of the wedge is one of them as it will collide against the upper walls of the gearbox housing. This means that the minimum angle is equal to the tangent of the free space between the wedge and the housing divided by the axial length of the ramp angle. Another limitation is that different cars have different shafts, these shafts have different lengths between the shafts universal joint housing and the gearbox housing (Denoted as X in Figure 4.11). It is important that the proposed disassembly tool works for all car variations.

4.2.3 Alternative Rings

A gearbox which was mounted in a rig to test the assembly and disassembly experimentally. A shaft would be mounted and different disassembly tools used to get it out. The initial hypothesis of the root cause for the shaft getting stuck was that the open ends of the ring get stuck between the male and female splines. To test this, a ring with a round profile and open ends bent inwards was tested (ring #2) from Figure 4.12.

Figure 4.12: Proposed ring and cross section

Figure 4.13: Damage on the shaft and ring after disassembly

Ring #2 was significantly harder to mount and the forces caused by slamming the shaft into the gearbox would move the entire rig some centimeters from the ground. When trying to pull the shaft out, it was completely stuck and left significant damages on the shaft as seen in Figure 4.13. The initial hypothesis that the open ends of the ring could get stuck between the splines was discarded since this ring did not solve the problem and other rings were tested. Radial rings which would be assembled perpendicular to the axis of the shaft were also tested but the only positive results was that they wouldn't hang loose. Other rings were slightly modified by reducing the OD, increasing the gap and bowing the rings. After testing over 20 different modified rings, ring #2 was the only one stuck.

Bowing them proved to be quite helpful and was significantly easier to dismount. It was also concluded that the best dismounting tool was the wedge while using a hammer with it. The lever worked in some cases but could start to bend when higher forces were required. Additionally, the lever was rested against the housing where internally, a conical bearing sits, which could cause a greater damage to the gearbox.

4.2.4 Inspecting Damaged Rings

Used rings which had damage marks were kept separately than the ones which had no scratches or visual signs of wear. From the ones with no apparent damage, 5 random rings were selected and measured the gap and in diameter every 30°. Results show that the average diameter was 0.75% smaller while the gap was 1.127% greater. This shows that rings without visual damages show close to no permanent deformation.

To correlate with the analytical approach, it was desired to find out where the dents were most commonly distributed on the rings. All the 17 damaged rings were positioned as in Figure 4.14 with the lower open gap at 0° and the dents pointing up. The position of the dents was then identified and logged. Dent locations were then plotted and can be seen in Figure 4.15. The average number of dents on the investigated rings was 6 and it was considered a dent when a major shear mark was seen on the ring. It is important to note that all the shear marks come from the contact side with the gear and never from the shaft which pushes the ring out. The distribution of the dent marks follows the pattern where the forces act on the ring as shown in Figure 2.5. Additionally, there was always small shear marks on the extrados at the open ends where the loads are considered as punctual. This shows that the contact on the open end is indeed punctual and is between the female spline edge and the rings extrados.

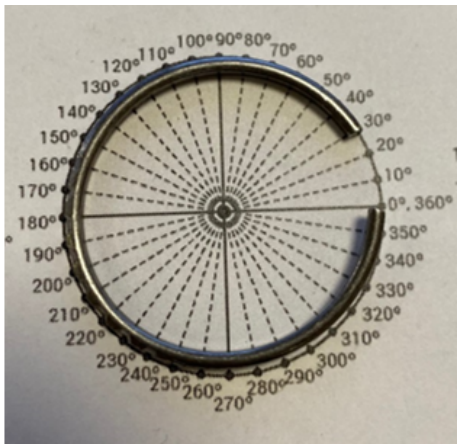

Figure 4.14: Positioning of damaged rings to log the angular position of the dents

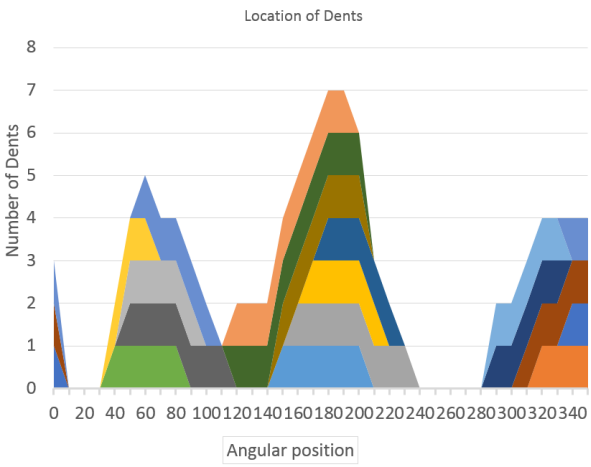

Figure 4.15: Angular position of the dents identified on damaged rings

Notice also that due to how the ring was positioned, there was never a part of the ring from 0° to 30°. The mode for this distribution was at 180° just as suggested by the analytical approach. The distribution also shows that the dents are usually located within the 3 regions with greatest contact. The damaged rings were also measured and the average diameters go between 95.5% and 102.5% the original nominal value. The gap was between 60% and 130% the original nominal value. This shows that once the ring gets stuck, they suffer higher stresses and permanent damage.

4.2.5 Benchmarking

Driveshafts from other cars in the market were inspected to see how they attach their shafts to the differential gear on the front left side and two different solutions were found. Audi Q3, Q5 and Skoda Karoq attach the joint with 6 bolts into a second half with an splined end. This half has a central bolt which keeps the splines locked axially as shown in Figure 4.16. This spline is lubricated and besides from

being a long bolt, it is unknown if the bolt has a positive locking mechanism to prevent it from loosening with vibrations.

The rest of the investigated cars on the market (Volvo XC40, XC60, Mercedes GLC, Volkswagen T-Roc, BMW X3 and Lynk & Co 1) also had a splined shaft with a snap ring. Only Volvo and Geely had an Oval profile on the snap ring, the rest had a circular profile and a radial ring. Most of the competitor cars also had grease in the splines which made the dismounting apparently easier.

Figure 4.16: Splined connection to the differential gear

Figure 4.17: Lever used to dismount the shaft and support against the T-Roc gearbox housing

Assembly and disassembly of the T-Roc was specially easy even with an improvised lever used as a dismounting tool. The gearbox housing offered a solid support to create a lever against and it only required a gentle push as shown in Figure 4.17. Grease may also have affected this results. Second easiest was the Mercedes GLC even when it had a separate differential box which was not fixed and would move on the floor. Both rings had a smaller diameter of about 2 mm and seemed less stiff when compressing the rings with fingertips. T-Roc and X3 had bent tips on the rings and barely any marks in the extrados compared to the used rings reported in Figure 4.15. Shafts from BMW, Mercedes and Volkswagen were tested and measured, results will be reported further on in this report.

4.3 Experimental Study

This section reports the most important experiments carried out in the UTM to test different parameters and obtain data, important parameters are identified to be

tested further on. Results from the identified mechanism which causes the variation in disassembly forces is reported here.

4.3.1 Setting up the UTM

The UTM used throughout all this study is a UCT 50kN located at Chalmers and calibrated 4 months before the start of the experiments. The experimental study will differ from reality as the input force is entirely in the axial direction and the pull out speed is only 3mm/min. It can also be argued that using the dismounting tool produces vibrations which could affect the dismounting of the shaft. This is similar to one of the tests performed on the interface to verify its functionality. Using a universal testing machine, shafts and gears were fixed as shown in Figure 4.18.

Figure 4.18: Assembly and disassembly set up in the UTM

In difference to reality, in this test, it's the gear which moves in and out and the test is done vertically instead of horizontally. The direction of the assembly however, is considered to make no difference as the ring sits deformed in the gears bore and gravity does not modify the test in any assembly direction. To set up the test, the shaft would be inserted in the gear without a ring to have both parts properly centered and then the shaft would be fixed in place. When moving up and down the gear, the vertical forces measured would not exceed 10 N meaning that both parts were centered properly and almost no contact would take place.

As the system is closed, there is no way to see where the ring sits. In order to start the test, the gear would be lowered to a certain distance and a click could be heard meaning that the ring expanded and sat on the bore. From then, the gear could be lowered less than a millimeter without any resistance until it would touch

both the bore wall and the shafts groove wall. From then, the tension could be started. The machine would yield 500 data points disregarding the test distance. Data had to be filtered manually to compare between the tests. To set the deformation as 0, the data would start as soon as a variation of 10 N or more was measured between two data points. This would then mark the reference point for all data sets and is considered to be where the ring first makes contact against the exit ramp on the bore. Meaning that all the plots would have a theoretical peak in the force at x = 0.8 mm where the ramp ends. Leading to a drop in the force as the ring is not blocked by the gear anymore and can slide freely. As the positioning of the gear to start the test is inaccurate, the peak forces were found at different places.

Throughout this study, over 300 data sets were obtained and compared, only some of them will be reported in this document. Figure 4.19 shows the disassembly of the same ring 5 times in a row without any modifications to the system. Peaks can still be seen at different places. Several different tests were performed with great variability each time. Many shafts, gears and rings were tested, the variability was the main issue in the study and can be clearly seen in the next Figure 4.20.

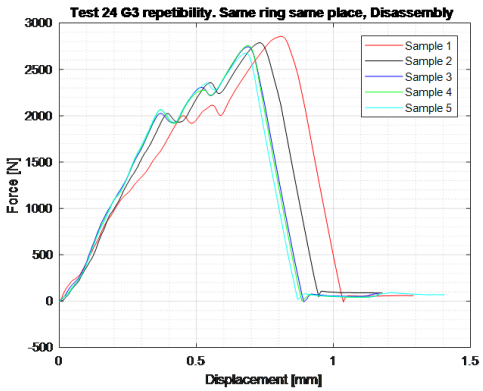

Figure 4.19: Repeatability test on disassembly forces for current rings

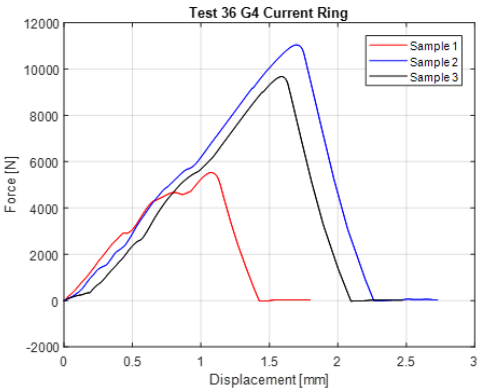

Figure 4.20: Variation comparison between disassembly forces

The plot shows disassembly forces for the current ring and can go up to almost 300% that of the allowed force. In other cases, the test had to be stopped to shear the shaft out using a hydraulic press as the ring was completely stuck.

4.3.2 Testing the surface roughness

To test whether or not the surface roughness could be responsible for getting the shafts stuck, a new gear (Gear 3) and the gear which had been used in numerous impact tests (P0) were tested and compared. Gear P0 was the one which showed high disassembly forces and was saved to test all possible rings, the surface on its splines was smoother as it was slightly worn from continuous testing. Results can be seen in Figure 4.21 and 4.22.

These forces are well within target and although there is some difference in pull out force between the gear, it is not significant. More tests were conducted and high peaks were identified in both gears and would reach up to 7 kN of force.

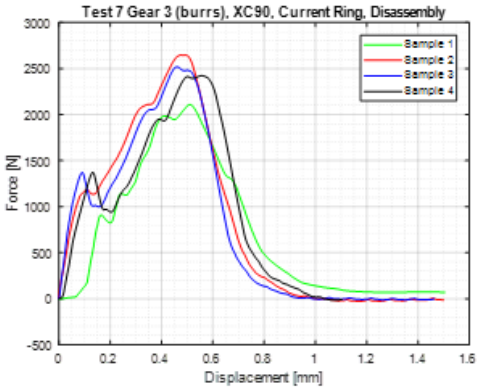

Figure 4.21: Disassembly forces on a gear with a rough surface

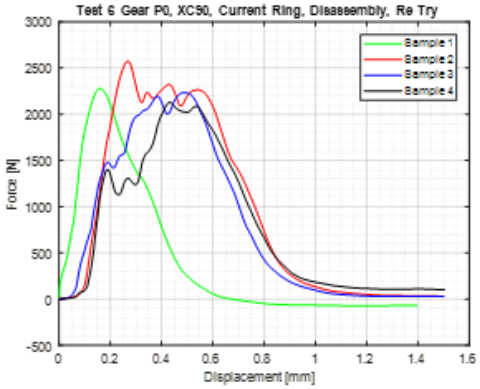

Figure 4.22: Disassembly forces on a gear with a smooth surface

To help reduce the friction coefficient, grease was applied everywhere in the gear and shaft. Although the grease helped reduce the force caused by the contact between the splines sliding, it showed no difference during the disassembly where the contact between the ring and the gear is hertzian, and even then a peak can be observed. It was then believed then that it was not the burrs but the ring itself getting trapped between the splines causing a locking mechanism. While most tests would average a pull out force of around 2.9 kN, it often happened that the force would spike up linearly until the ring was sheared and the force would drop. In contrast with tests with uneven slopes where the ring is believed to slide freely causing the unevenness in the curves as can be seen in Figure 4.22.

4.3.3 Identifying the Locking Mechanism

As seen in the Tolerance Study, there is a possibility that the ring closes on a spline or getting trapped between the male and female spline creating a locking mechanism. Additionally, the female spline lacks two splines, therefore it was tested whether or not it was these gaps which caused the rings ends to stick in and cause the locking mechanism. Rings were tested at different angular positions but results show force peaks disregarding the tested angular locations. Meaning that the locking mechanism does not only occur when the open ends are positioned against the missing splines on the gear.

To further test if the rings ends gets trapped between the splines, the ring was positioned with the open ends where the female spline would have contact with it as shown in Figure 4.23. For the next test, the ring was then rotated half a spline, where the male spline (shaft) would be in contact with the open ends of the ring. Note that the ring never rotates during the test, as the contact is done at low speeds,

once the contact is established, the ring is locked in angular position. Even after disassembly, the ring remains in the same place. Results can be seen in Figure 4.24 and 4.25

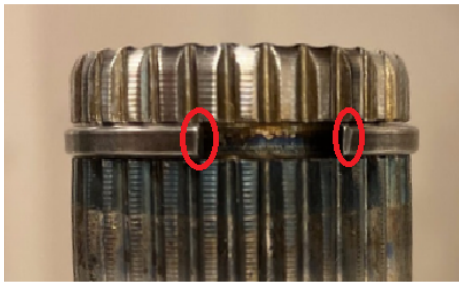

Figure 4.23: Positioning of the ring against splines on the gear

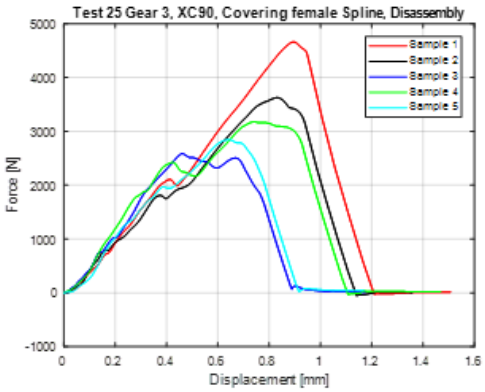

Figure 4.24: Disassembly forces when ring is positioned towards gear splines

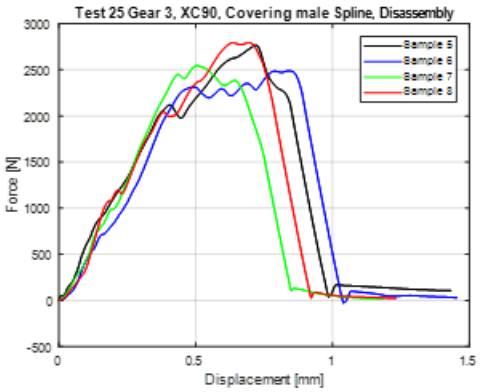

Figure 4.25: Disassembly forces when ring is positioned towards shaft splines

Results show how the ring with open ends which has contact with the splines on the gear presents force peaks. On the other hand, positioning the ring against the shaft splines had much lower variability. The same test was ran using different gears and shafts and results show the same outcome. Rings got stuck disregarding which spline they faced at when inserted into the gear but tests show that with a gap of 11 mm, rings were more prompt to get stuck when facing at the female splines. This may be because the positioning was not accurate but could explain that the variation is just a matter of probabilities.

To try to prevent the open ends getting stuck, many tests were developed. Rings would be modified as in Figure 4.26 and 4.27 to create a sliding motion between the ring and the gear splines. Although less samples showed peak forces, this meant that the major cause of the variation was still present.
To eliminate the supposed mechanical locking between the tips of the ring and the splines of the gear, a ring was modified bending its open ends inwards. This solution had been previously disregarded since one of the rings proposed by the supplier

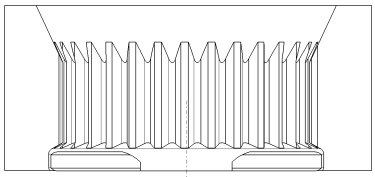

Figure 4.26: Modifications on the tips of the ring

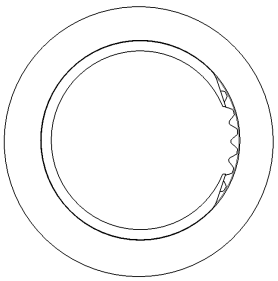

Figure 4.27: Modifications on the tips of the ring

(ring#2) even sheared some splines on the shaft. However, new attempts at this test gave a low force variation and the lowest pull out forces yet. Some of the samples still showed high forces and is believed to be because the bent tips were bent inwards too much. The tips have a direct contact with the shaft and try to "dig" into the shaft when the ring was compressed. Physical marks could be seen on the shaft's groove bottom.

Previous test results don't correlate with the results from alternative ring #2 tested previously, where tips were bent inwards to prevent them from getting stuck and still sheared off the shaft splines. This ring was tested on the UTC to obtain data and showed that the open ends also try to dig into the shaft. The radial thickness of ring#2 is slightly larger than that of the current ring. The gap between the shafts groove and the female splines is just enough for the radial thickness of ring#2. Meaning that most of the rings intrados had to be in contact with the shaft's groove bottom to allow the disassembly. As the open ends were bent, this created an angle which required a lot of force to unbend. The bending on the open tips would then stick out and contact the female splines locking. Additionally, the open ends would not be able to slide and deform as they were digging into the shaft.

Further testing of modified rings finally got the assembly stuck, where a ring with ends bent outwards peaked around 14 kN and the whole jig was starting to deform. The shaft had to be pushed out using a hydraulic press and the ring showed 5 holes where the splines sheared through.

It was also believed that dents caused by hammer strikes to unsuccessfully remove the shaft would make it harder to dismount as the dents would also act as a locking mechanism. The same ring from the disassembly method #3 which showed significant dents was placed in the UTC machine to see how this would influence the disassembly forces. Results can be seen in Figure 4.28.

This plot shows unnatural forces to disassembly the ring and it can be noticed on the smoothness of the curves where the force increases constantly until a drop. The plot shows that using brute force to remove a ring without managing to deform it but instead, shearing it and creating dents, causes a bigger disassembly challenge later on. The dents formed by the hammer hits, lock to the splines and block it from

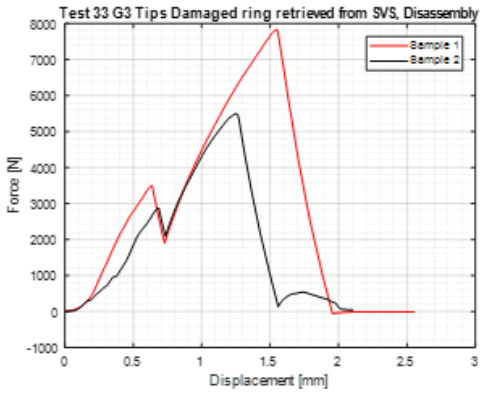

Figure 4.28: Disassembly forces from a damaged ring

sliding, resulting in huge disassembly forces. This means that using brute force to get the ring out is not the solution as it may lead to greater disassembly issues and damages the parts in the process.

From the analytic study it is understood that the contact between A-B is constant as the ring slides. On the open ends however, as the angular width increases due to the deformation and the gap starts to become smaller, the contact between the ring and the gear varies. A ring was painted and the disassembly test was performed. Figure 4.29 shows how the contact close to the open ends is not axial but becomes almost tangential. This is because the ring has to slide through the ramp angle in order to contract and at the same time, the open ends move angularly closing towards each other. When the ring has dents, the angular movement gets locked as the splines fit the dents and no axial sliding is allowed. This experiment also proves that open ends can close on a spline. If the contact between a spline is far from the end of the ring, there won't be any radial forces pushing the very end of the ring inwards. The open end will then close on the walls of the adjacent spline as illustrated in Figure 4.6.

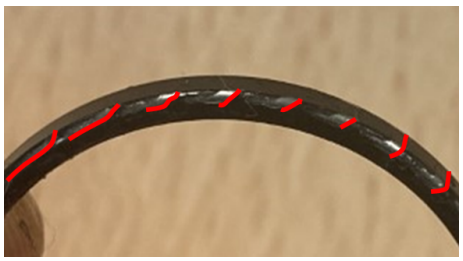

Figure 4.29: Contact marks on the surface of a ring after testing

4.3.4 Reducing the Pull out Forces

After having understood what seemed to be the source of the force peaks, more parameters were tested to see which ones would lower the disassembly forces the most. From the previous experimental study, the bowed rings were quite easily removed and hence were tested next. Although some curves show slightly lower forces compared to previous tests, it still shows peaks in some cases. It is believed that as the ring is slowly compressed, both ends align and the miss match between the open ends is lost, resulting in a regular ring.

From the analytical study and the formula from [8], it was found that with the lower angular width, the lower the radial force for the ring to exert against the housing. This was tested experimentally by cutting the ring into a certain angular width (increasing the gap). Disassembly forces showed smaller variations and maximum forces were reduced as the gap was increased. Figure 4.30 shows how forces were lowered considerably in most samples however, the mechanical locking is still present and peaks at only 2.7 kN.

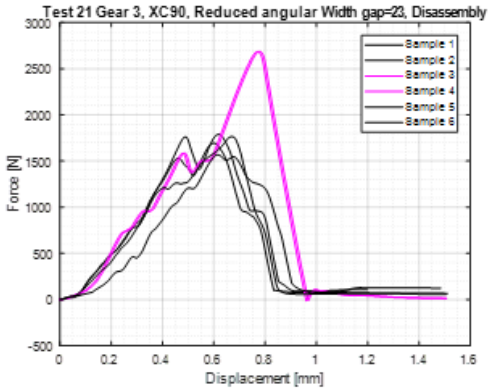

Figure 4.30: Disassembly forces on rings with a gap of 23 mm

By reducing the angular width, the contact and the deformation needed by the ring is reduced. Previous test showed positive results in disassembly forces but had the ring hanging loose which is not desired. Hanging loose could create more problems in the future if the part is in contact with a face which does not have a ramp angle, meaning a very deep bore or the face of the gear perpendicular to its axle. This feature has also been previously identified and should be avoided.

To reduce the contact against the gear splines and have the ring sit tight in the shaft, the ring has to be changed from axial to radial. The open ends can then be bent inwards to have a contact with the groove bottom while avoiding them to dig in during deformation. In this way, the open ends are less likely to get stuck into a spline. Considering this, radial rings with an oval shape were made by bending the current ones.

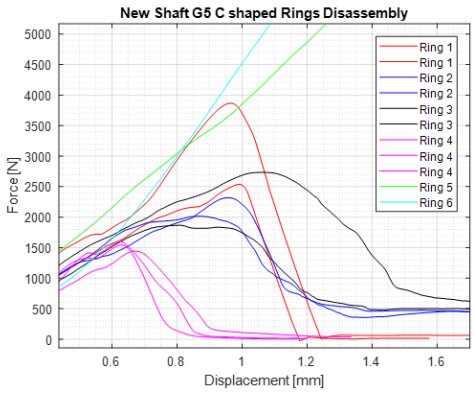

Figure 4.31: Disassembly forces on different oval rings

The results from the previous test shows that the forces are almost too low. Rings show contact marks with only three splines: at the largest diameters and at A. Rings 5 and 6 had their open ends in contact to the shaft, causing them to dig as seen in previous tests. Ring 6 ended up losing its ovality and had shear marks all along its periphery.

4.3.5 The Ramp Angle

From the analytical study the ramp angle was identified as a determinant factor on the axial force needed to pull out the shaft. Since the splines on the gear had been previously hardened, there was no easy way to machine a new bore in them. A new set of gears was modified using a grinding stone to create a new ramp angle of 60.5° and 57°. One of the stones used can be seen in Figure 4.32.

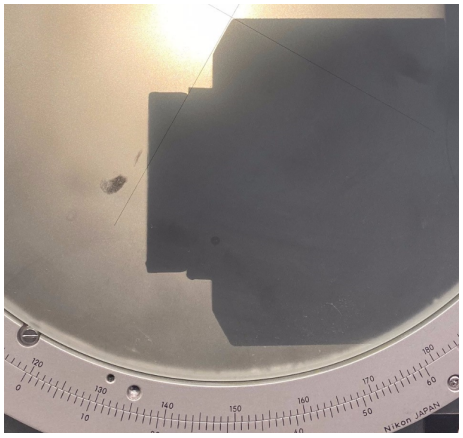

Figure 4.32: Grinding stone with an angle of 119.5°

Some of the existing splines were destroyed and therefore the length of the spline contact was modified. However, since the splines show no interference between each

other, this change should not affect the force measurements from the tests. The surface roughness left from the grinding stones was also quite smooth due to the nature of the manufacturing process.

Most of the following tests had constant high forces and peaks. The shaft showed some visual damages and was therefore measured. The shaft had an angle of 4° caused by the continuous testing while a new shaft should have 0°. This may have been the reason why the shaft showed higher forces than when using a new shaft as the axial force is not constant on the ring. Throughout all the testing, this happened to three shafts. Shaft from Figure 4.34 left dents on the rings at the same place as the shaft was damaged, which can be seen as the black area between the ring and shaft.

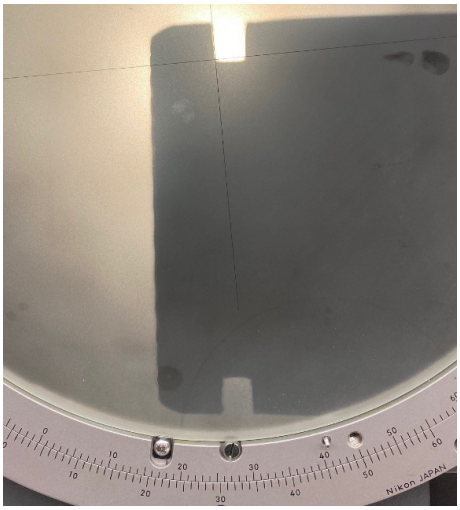

Figure 4.33: Damage on the groove walls of the second shaft

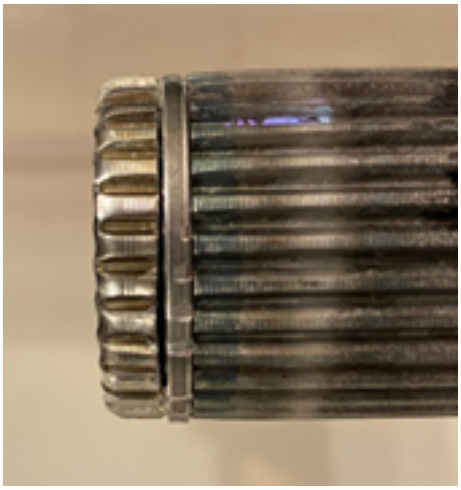

Figure 4.34: Visible damage on the third damaged shaft and dents on the ring

The amount of shafts used throughout the testing was limited and all were tested more than once. Damage was only seen after a ring was stuck and axial loads would go up to 10 kN or more. To make the shaft more sturdy against these loads the formulas from the manufacturers handbooks can be applied to make the shoulder width larger. On the other hand, this would be unnecessary as space in the differentials is often limited and with a proper ring design pull out forces wouldn't be so large. What was noted is that by not having a perpendicular contact to the ring or by not having a constant contact with the ring, the pull out forces escalated considerably. This was even the case with rings which had previously showed low disassembly forces.

With a new shaft, the ramp angles were tested again. Even though some results showed lower values in the disassembly forces, the tests still showed a lot of variation and even got stuck, meaning that the ramp angle alone wouldn't solve the problem. The proposed oval rings where then tested and showed too low forces. The peak axial forces can be averaged by taking only the experiments in which the test is not

considered as stuck, meaning that the slope does not increase linearly and higher than 4 kN. This average is not applicable to reality but it is applicable to a design where the locking mechanism does not occur and the rings don't get sheared off during disassembly.

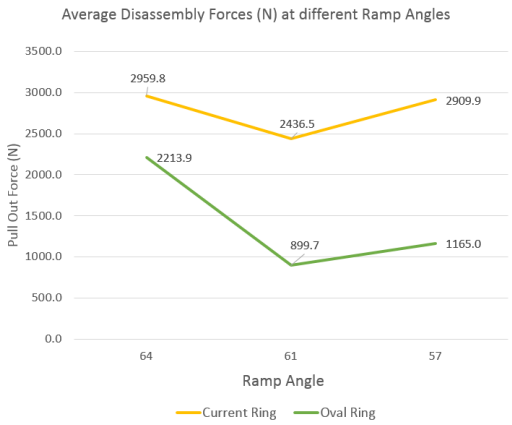

Figure 4.35: Average pull out forces for different ramp angles and ring designs

Results from Figure 4.35 show that the forces increase from a ramp angle of 61° to a ramp angle of 57°, this can only be explained due to the high variation between one test and another. To get more realistic data, the test would have to be performed many more times (in this case only 4) to obtain a statistically trustworthy result.

4.3.6 Testing Benchmarked Interfaces

The shafts and gears previously stored were tested in the universal tensile machine and measured. Forces show considerably lower pull out forces and less variation; all with a round profile and a radial ring. Ramp angles and surface roughness are reported in Table 4.2. It is worth pointing out that the surface roughness measurements were not taken according to standards and only one spline was measured. The diameter on the cross section of the rings was between 1.8 and 2 mm.

Table 4.2: Table comparison between interfaces and disassembly force

	Volkswagen	**BMW**	**Mercedes**
Ramp Angle (°)	60.2	54.7	55.6
Surface Roughness (Rz)	19.53	6.33	12.55
Spline Modulus and Number of Splines	0.75, N = 36	1.5, N = 27	1, N = 24
Disassembly Force (N)	1,250	1,500	1,100

Table 4.2 supports the claim that the surface roughness is not the main factor which determines the disassembly forces but may cause an interaction between other fac-

tors. Even with a higher surface roughness than the current ring samples, the disassembly forces are significantly lower and the force never peaked due to the ring being locked. Note also that with the spline modulus increasing, the forces also increase, this is because longer teeth require a larger deformation on the ring.

Gears tested earlier on were also measured. The ramp angle measured on the gear P0 was of 62.1° and therefore out of spec. Although it could have been the constant testing what modified the ramp angle on the gear. The ramp angle could explain why this gear was the easiest to dismount, however P0 was one of the first gears to get the shaft completely stuck. The surface roughness of this gear was smoother than the rest because of the numerous tests performed on it, smoothened its surface as shown in Figures 4.36 & 4.37.

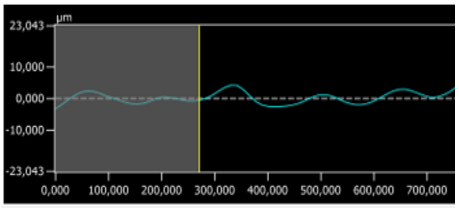

Figure 4.36: Surface roughness on gear P0

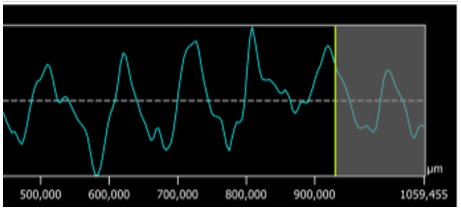

Figure 4.37: Surface roughness on a new gear

4.3.7 Testing Cross Sections

The cross section of the rings was also tested by grinding away some material, rounding edges and testing a round cross section. All of these tests also got the rings stuck at least once. Even when reducing the cross section significantly and ending up with a ring which was easy to deform radially. The variation in these tests was even larger and therefore will be further tested in the computational model.

Having tested different surface roughnesses, ramp angles and shafts; results shows that the factor causing the most variation in the tests is the geometry of the ring. Reasons being the excessive contact between the ring and the splines and causing the possible mechanical lock which blocks the ring from sliding tangentially to the splines. Although other parameters do affect the disassembly forces, the oval ring design will be tested further using the computational analysis. The cross section of the ring will be further investigated as round because even if round is more stiff than the current profile, it can be optimized to get the right measures. Another reason being that in case that the ring gets stuck, the round ring will be sheared off easier. Lastly, the round profile avoids doesn't have any sharp edges as recommended by [13] and the normal forces on the contact would turn radial faster.

Figure 4.38. shows in brown, the comparison of the cross sectional area that would need to be sheared in case that the ring gets stuck. Although the round design requires a deeper groove on the shaft, it saves up some axial space on the shaft. In

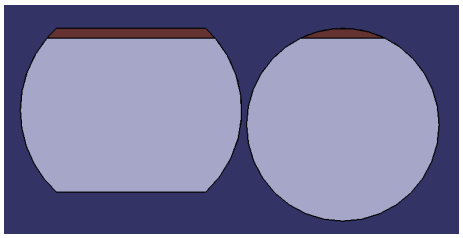

Figure 4.38: Comparison between area needed to be sheared off in two cross sections

addition, this design has less chances of getting stuck during assembly or disassembly when pushed against corners, this has been previously identified as a risk and should be avoided.

4.3.8 Dynamic Testing

With the objective of comparing the forces obtained during static testing with the real disassembly forces transmitted through a disassembly tool and a hammer, the following experiment was developed. A body with a known weight would hang freely on a string and would act as a pendulum. The pendulum would be released at a new known distance and impact the wedge perpendicularly. The whole process would be filmed with a high speed camera to see how much distance the wedge traveled. The potential energy can be calculated from the two heights and the impact force can be obtained using the work energy principle, in this way (4.10) is obtained.

$$KE = mgh \rightarrow F_{impact} = \frac{E}{D} \rightarrow F = F_{impact} cos(\alpha_w) \tag{4.10}$$

Where KE is the kinetic energy, E is the total energy, D is the distance the wedge is pressed in between the housing and shaft and α_w is the wedge angle. This experiment is under the assumption that all the energy is transferred into the impact and the impact occurs at the lowest point in the pendulum, where there is only kinetic energy. Notice that the experiment can not give very accurate results, due to the impact not being perfect or perpendicular, the wedge by not having the perfect contact and other reasons. However an operator is able to use the wedge and a hammer with much more precision than a pendulum hitting a wedge hanging loose. Meaning that results should not give higher forces than in required in reality. The following figure shows the moment the pendulum hits the disassembly tool.
The tests which required the minimum potential energy on the pendulum are reported in Table 4.3. If a shaft was removed successfully, the potential energy of the pendulum would be reduced for the following test until the impact wouldn't be strong enough to dismount the shaft after four attempts.

The same test was performed in the gear with a modified ramp angle of 57°. The results don't show a big difference as the minimum potential energy registered was very similar. What is important to notice is that the shaft was very easily released

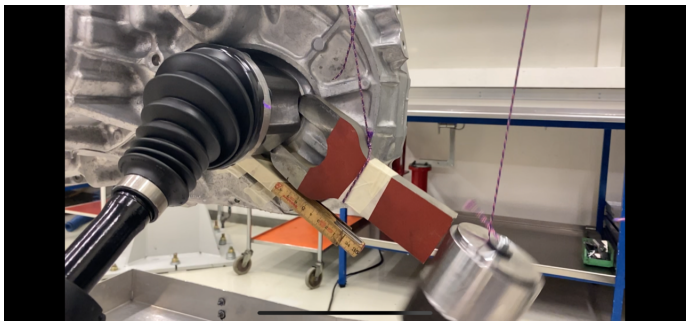

Figure 4.39: Instant when the wedge tool is hit by the pendulum during Dynamic Testing

Table 4.3: Results from the lowest values obtained during dynamic testing

Ramp Angle = 64°	**Current Ring**	**Oval Ring**
Weight (N)	39.73	39.73
Height at Release (mm)	1110	900
Height difference (mm)	325	115
Impact Displacement (mm)	5	5
Potential Energy (N*mm)	12912.41	4569
Impact Force (N)	2582.48	913.8
Wedge Angle (°)	25	25
Axial Force Generated (N)	2340.52	828.18

using a lever and a slight pull with the hand. This shows that even if oval rings may solve the problem of rings getting stuck, they could be released with too much ease, because of this it is important to perform a DOE to obtain the optimal parameters.

Forces registered in the dynamic experiment are smaller than in the static testing, meaning that as long as the ring does not get stuck, obtaining a value of about 2.5 kN in the static test, the design should be possible to dismount using a wedge and a hammer. An interesting conclusion is that, with a robust design of the snap ring, both a lever and a wedge tool work well. The lever will not bend nor cause too high forces against the gearbox housing so either disassembly tool can be used depending on availability and working space.

4.4 Computational FEM model

Based on [15] a good insight was obtained on how to set up FEM simulations in ANSA. The model is then processed using Abaqus solver and results can be later analyzed using Meta post processor or Hyper Viewer. The simulation tries to simulate the assembly and disassembly mechanism of the shaft, gear and snap ring; to do this an implicit non linear simulation was used. Once a base model is set, the pull out forces will be compared with the ones obtained in the experimental testing to make sure the output from the model is within expected values. After the model has been correlated with reality, a DOE will be performed using the proposed oval

rings and find the optimal parameters for the factors which could not be tested in the experimental testing.

4.4.1 Friction Estimation

In order to obtain a value for the friction coefficient between the ring and the gear, data from the experimental study was analyzed. Axial forces measured when the ring is fully compressed and is sliding through the female splines of the ring would be the result of pure friction between the two bodies. The axial forces can be then used to obtain a friction coefficient for the computational model. These values are compared to the ones proposed by [17]. Figure 4.40 shows the insertion force when the ring was pushed at its mean diameter with a metal rod avoiding any contact to the gear.

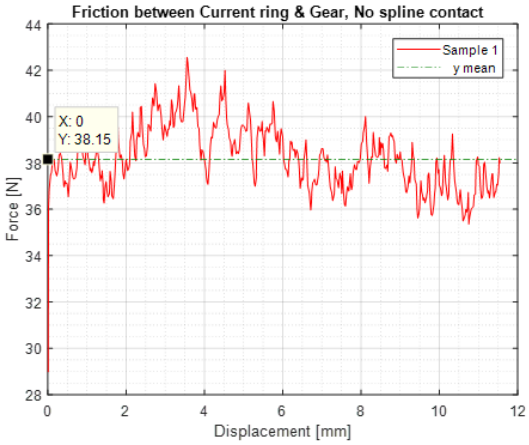

Figure 4.40: Friction forces acting on a fully deformed ring sliding through the gear minimum diameter

With a mean value of 38.15 N, this will be taken to estimate the friction coefficient between the two parts. This graph also shows that the contact between the shaft and the gear results in an axial force equivalent of about 15 N. Proving that the shaft and gear were quite well axially aligned during the experimental testing. The friction forces will be proportional to the radial forces acting on the gear splines which are keeping the ring deformed. These forces have been previously estimated analytically using 2.6.

$$F = R * \mu \rightarrow \frac{38.15}{338.82} = \mu = 0.112 \tag{4.11}$$

The base coefficient for the FEM simulations will then be $\mu = 0.112$. It can be argued that the surface is less smooth at the ramp angle meaning that the coefficient should be higher. However, the assumption used to calculate the radial force is not accurate and higher radial forces are present in reality resulting in a smaller friction coefficient. While the book [17] proposes a range from 0.1 to 0.3 between two steels, the friction coefficient will be taken as a base for the FEM model and modified if needed.

4.4.2 Deforming the Ring

In order to obtain a more accurate value for the radial force needed to deform the ring with the worst possible tolerances enough to pass through the gear, a simple FEM model was developed. The model was made in ANSYS due to its simplicity. The simulation consisted of a housing which would deform radially, using cylindrical coordinates until the diameter of the gear. A contact was set with half a ring and both bodies would have a frictionless support to simulate symmetry. The mesh was done in hexahedral (hexa) elements and a friction coefficient of 0.112 was used.

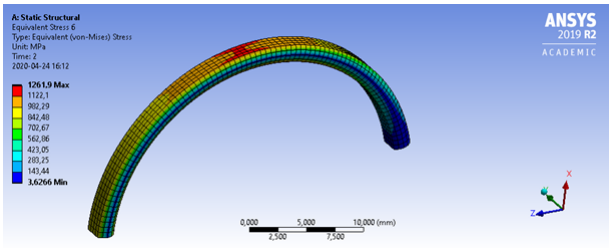

Figure 4.41: Von Misses stresses acting on a deformed ring

The stresses on the ring would reach up to 1,260 MPa mostly from bending stresses between B and C. While the localized frictional stresses at C would go even higher. This is different than what was expected from the theoretical study where the highest stresses were expected at A. Separation could also be seen in this simulation by adding a contact tool. As predicted in the analytical study and observed during assembly. If the radial displacement was placed on the ring, the radial reaction forces could be obtained and would be comparable to those from the theoretical study as they were applied constantly along the rings extrados. The force obtained was 173.3 N for half a ring, meaning that for a full ring, the radial force needed would be 346.36 N. This force was close to 2% different to the one estimated earlier. The difference with reality, is that the force is much higher as it is localized at A-B and as a punctual load at C.

Attempts to increase the complexity of the assembly simulation were done in ANSYS but often ended in non convergence. For this reason, this model was abandoned and moved on to ANSA.

4.4.3 Basic Assembly Model

The model consisted of three parts: the gear, the shaft and the snap ring. The objective is to simulate the assembly and most importantly, the disassembly of the shaft. To do this, a displacement is placed on the shaft until its groove matches the bore on the gear. The snap ring then has to engage a contact with the inner surface of the gear and deform while its being pushed by the shaft. When the snap ring matches the bore it will be allowed to expand and lock the system. From this point, the shaft would return to its original position simulating the disassembly. To model this, an implicit, non linear simulation was performed using ANSA and solve

the model using Abaqus.

From recommendations from the CAE department at VCC, it was best to start from a simple model and start building in complexity to get familiar with the software, the model building and some common errors. This model however, does not give any accurate data as the shaft has to be smaller than the gear causing pure shear forces on the ring. In reality, splines act as opposing forces and cylinders cant model this without overlapping themselves. Based on the original geometries, a static nonlinear simulation similar to [15] was developed.

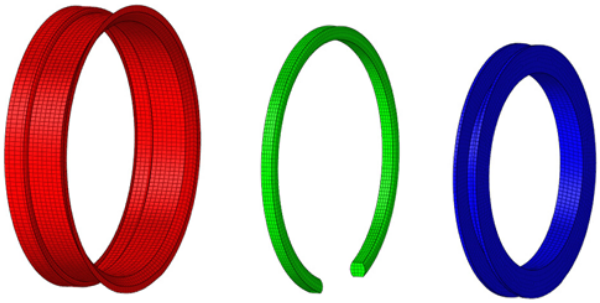

Figure 4.42: Simplified parts

Figure 4.42 shows the exploded assembly, where the red body is the gear, considering the inner surface of the gear and shortening it. The green body is the snap ring in the biggest possible measurements according to tolerances. The blue body is the shaft where the displacement would be placed, pushing along the snap ring into the gear. As geometries were quite simple, everything was meshed in hexa elements and both the gear and the shaft were made rigid using the Abaqus window in ANSA. The simulation would consist of two steps, the first one where the shaft is pushed into the locking position and a second one where the shaft would be pulled out and the ring would have contact with the ramp angle. Once the input file for Abaqus was generated using ANSA, it would be solved in the VCC cluster and results would be analyzed using Hyper Viewer and Meta post processor. Even though pull out forces where around the expected values, the model was too simplified to give any relevant data.

To reduce computing time, a symmetry boundary condition and the pull out forces were expected to be halved. While the symmetry did reduce the computing time considerably and the forces were as expected, the idea was scrapped as the splines on the gear are not exactly symmetric.

4.4.4 Splined Model & correlation

Once the basic model was working, it was time to model the splines as they have very different loads than the simplified model. The shaft and gear were shortened since there was no need to have the ring slide throughout the whole length increasing the number of elements in the model. Since the experimental tests failed to show

any big differences when positioning the ring against the missing splines, this feature is not implemented in the models. It is however, reviewed later on in this report as time allowed to perform some extra simulations. Considering that the gears never showed any physical damage during all the experimental testing, they were kept as rigid bodies as in the previous model. Shafts were also kept rigid because they would only be damaged after shearing the ring and taking heavy loads. Additionally, earlier tests with flexible bodies had very long computing times of over 40 hours per run since this contact simulations required up to 1,000 increments per step. The geometries are shown in Figure 4.43.

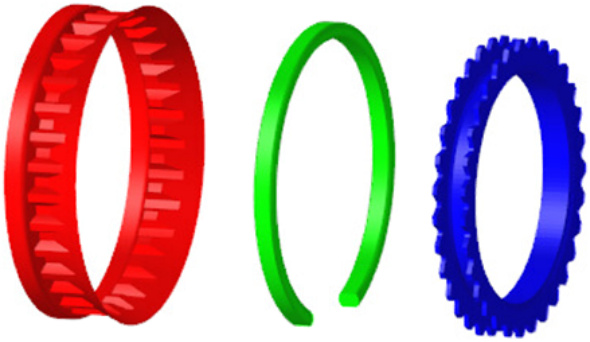

Figure 4.43: Mesh for the splined model in hexa elements

Due to the simulation relying on the contact pair established between the three bodies, convergence was not always achieved and some models would remain in the same position even after the 1,000 increments and a contact stabilizer. An input from the CAE department was that rigid bodies mustn't have second order elements nor hexa elements. To make the meshing simpler, tetrahedral (tetra) first order elements were used for the rigid bodies. The ring which is the only flexible body was still meshed using hexa elements to help achieve convergence in the contact.

To prevent contact between the spline and the gear, a contact exclusion was added in between the splines for the first model. To be able to modify geometries in the model faster, the shaft was scaled down to 99% of its size in relation to its center. This simplification meant that there was always a very slight gap between the two bodies as the displacement is strictly through the axis.

To correlate the results to reality, the assembly step is compared first as the contact was easier to converge. The basic model had a shearing effect on the ring and therefore showed some high loads compared to the splined model. As mentioned before, the basic model yields irrelevant data, it was only shown in this report to prove the symmetry worked and could be implemented in future simulations.

Figure 4.45 shows that the symmetry condition works quite well when the model is entirely symmetric. The assembly of the splined model shows that the force jumps from the start, this is because the contact was placed before the simulation

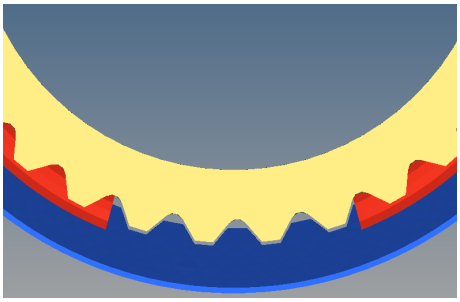

Figure 4.44: Scaled down shaft to avoid contact

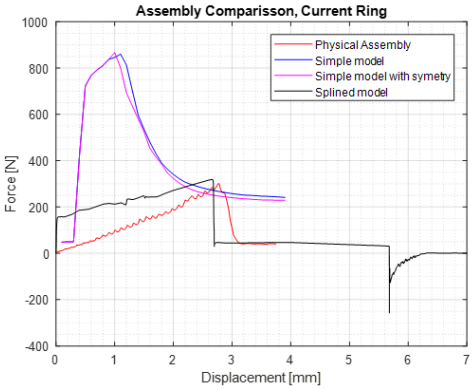

Figure 4.45: Assembly forces from simulations vs reality

started. The max force is the important aspect here and can be seen quite close to the physical experiments in the tensile machine. This model used the theoretic friction coefficient estimated earlier in the report. It is important to notice that after the ring enters the ring, the force is also quite close to the experimental test, around 40 N and then drops when the ring enters the bore and springs back to shape.

It was common to have non convergence even after 1,000 increments in one step. This was caused by very sharp contacts between the meshes as can be seen in the red element in Figure 4.46. To solve this problem, the nodes on the open ends of the ring would be moved manually about 0,1 mm inwards to create a better sliding motion as shown in 4.47. This helped converge the model in many cases.

In the first simulations during assembly, the stresses on the ring were much higher than the yield strength used. At first an unhardened steel was used for the ring, this resulted in permanent deformation on the ring which made the outer diameter smaller after assembly and made the disassembly easier showing wrong pull out forces. The material was then adjusted with a yield strength strength of 1,420 MPa according to the supplier's input. This stress is rather high for non heat treated steels and would suggest that if the heat treatment is not proper, the ring would have a permanent deformation. Hardening the ring is also suggested because it

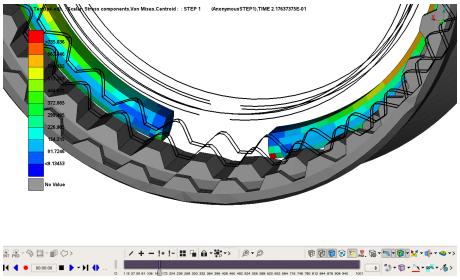

Figure 4.46: Non convergence contact

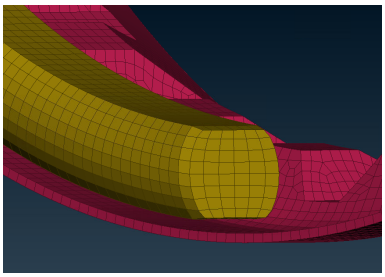

Figure 4.47: Modified open ends to help achieve convergence in the simulations

would make it harder to create dents on the extrados which can act as a locking mechanism as seen earlier in the experimental testing.

Stresses on the ring are even higher than the ones estimated in the simple ANSYS model and go up to 1,441 MPa although very localized in the contact regions. While in the area between B and C, the stresses are almost as predicted in the ANSYS model. Again, it can also be seen that the maximum stress is caused by the bending and can be found when the ring is deformed the most. This also correlates to what [8] predicts on the behaviour of thin rings.

It is important to notice that the maximum pull out forces are generated before the maximum deformation on the ring. This may be due to normal loads being closer to the horizontal and thus, opposing the pull out as shown in Figure 4.48. This is another reason to change the profile to a round one as the normal load would start to turn vertical (radial) faster with a reduction in diameter. Reducing the diameter on the cross section of the current ring would reduce the moment of inertia and its stiffness too much before having any effect on the angle of the normal force.

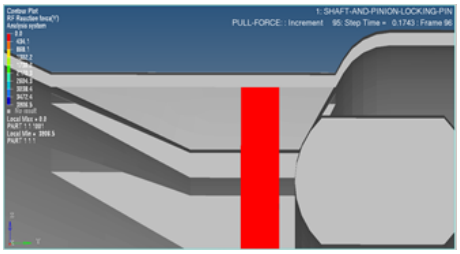

Figure 4.48: Maximum axial force registered

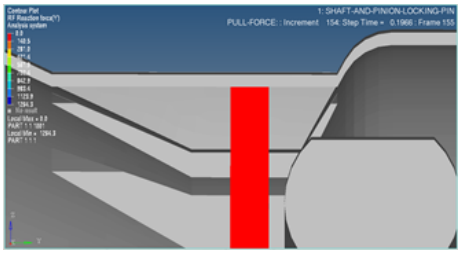

Figure 4.49: Axial force decreases to get maximum deformation

The pull out forces were plotted and compared to one of the physical experiments on the current ring. Notice that the pull out forces had a peak average of about 2,9 kN from all the tests, however the chosen test correlates quite well to the simulation. Variation may be explained by reducing the friction coefficient as it acts as a scale factor on the pull out forces. This big difference was opposite to the physical tests where a smoother surface wouldn't show that much of a difference in pull out forces.

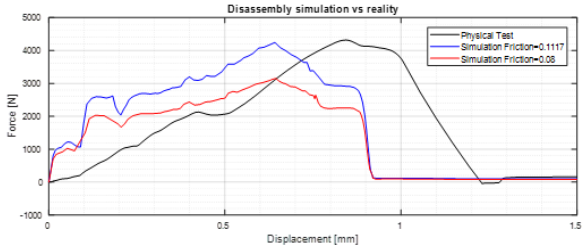

Figure 4.50: Comparison between pull out forces in reality and simulation

4.4.5 Verifying Assumptions

In order to verify whether or not there was a difference between pushing in the shaft or the gear in the experimental phase, the displacement was set on the gear and the shaft was fixed. Forces obtained were identical and curves would get entirely overlapped so results won't be shown in this report.

Angular width of the ring was also modified in one factor at a time experiments and pull out forces were considerable modified as shown in Figure 4.51.

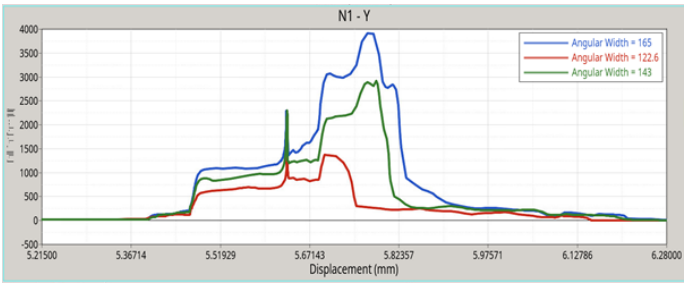

Figure 4.51: Disassembly forces on rings with different angular widths

Another test performed was to rotate the ring 1 degree at a time to see if this would make any difference like in the experiments with the UTM. Results didn't show any significant changes as the forces would vary by about 6%. This variation was most likely due to the angular position of the gear and the open ends of the ring not being at the very edge. This test did not show any mechanical locking but it may also be because the gap used was always nominal and never came even close to touching or being small enough to catch one single spline. Results from this experiment correlate quite well to experiments made in the UTM and the theoretic study. It also shows that in order to reduce the pull out forces, the geometry of the ring has to be modified. The problem with reducing the angular width on the ring is that it will hang loose, to solve this the oval design will be inspected further.

Once the model was as close as the author managed to get to reality and due to time limits, the DOE was started.

4.5 Design of Experiments

In this section, the results from the DOE performed to the oval ring designed based on the learning from the previous studies. The information was processed using Minitab in order to understand which parameters affect the most the axial forces during assembly and disassembly. Basic assumptions were made to reduce the size of the factorial.

4.5.1 Scope and Basic Assumptions

From the experimental approach, many parameters were tested and hypotheses were formulated. Using a computational model allows to modify the rest of the parameters in the interface. The proposal on the final interface design will be based on the results from the parameter study as the source of the huge variations is suspected to have been identified during the experimental study.

"Conceptually, the simplest method to sensitivity analysis is to repeatedly vary one parameter at a time while holding the others fixed" [14]. This is not optimal in complex experiments because the interactions between factors are ignored. Trying to test out every possible parameter in the model would yield an infinitely large factorial. For this reason, a factorial with 4 factors was developed. From the original parameter matrix some were already tested in the experimental studies and some assumptions were made to simplify the factorial.

Spline size was left unchanged as it would require a bigger research to be conducted in order to prove that the functionality is not affected. The shaft groove depth was also left unchanged because increasing it may affect the strength of the shaft creating a bigger problem. The ring design was changed into a radial ring as explained previously, this also eliminates the gap of the open rings as a factor since the goal is to have them tangential to the shafts groove to allow a sliding motion. In addition, the ring wouldn't hang loose on the shaft. The design of the new ring is illustrated in Figure 4.51.

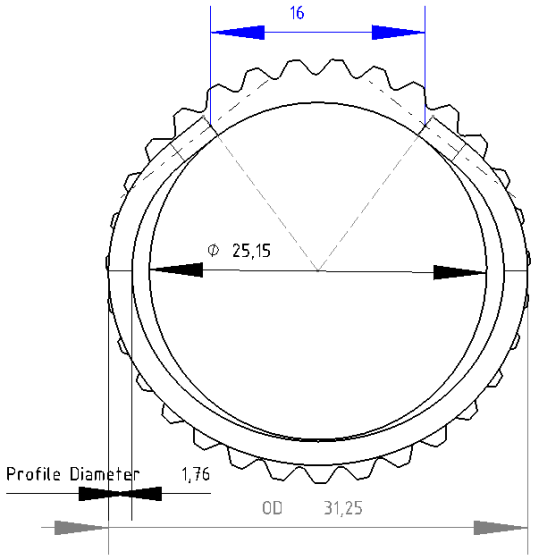

Figure 4.52: Oval ring design and parameters in the DOE

The distance on the open ends was set to 16 mm from the normal axis of the ring, reason being that during experimental testing, this gap allowed the ring to easily

assemble radially. Moreover, this gap allows tangency to the shaft surface and leaves about 1 mm of the open ends after the tangential contact with the shaft. The purpose is to prevent manufacturing tolerances from having a too short ring and allow it to dig into the shaft.

The parameters to be changed in this study are then the maximum outer measurement on the ring (OD), the profile diameter of the ring, the ramp angle of the gear and the friction coefficient μ.

4.5.2 Modifying the Model

Based on the previous FEM models, the new geometries are added to the model and meshed using the same element length. Note that since the initial contact is set before the simulation starts, the total displacement of each experiment will be different, depending on the OD of the ring. Simulations tended to diverge, for this reason, the ring was also meshed using tetra elements and then modified to quadratic elements. This new mesh helped the models converge significantly.

The new oval design shows more localized contact pressures with only one or two splines at a time and requires less deformation. In comparison with the previous round ring which had contact with many more splines and required more deformation. Additionally, the oval ring deforms almost entirely vertically with a small sliding contact located on the open ends of the ring and the shafts groove bottom. In contrast, the current round ring has the sliding contact against the gear splines, and as shown earlier, a small dent in the ring could get it stuck.

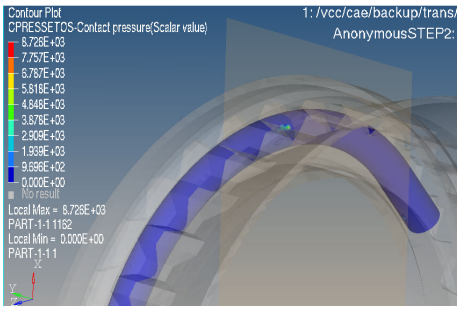

Figure 4.53: Contact pressure on the oval ring

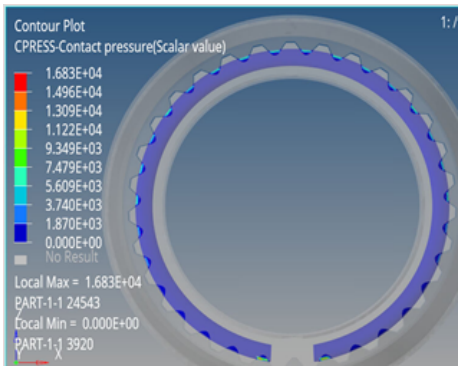

Figure 4.54: Contact pressure on the current ring

The contact pressure contour plots show where the dents should be located on the two ring designs, which is exactly where they were found during the experimental testing in the UTM.

Stresses may rise above the yield limit of the current heat treated steel, but only on very localized areas due to shearing loads and show where the dents would be located. On the rest of the ring, stresses are increased as the OD on the ring grows

Table 4.4: Factor design table

Factor	Name	Low	High
1	**OD (mm)**	31.25	33.5
2	**Profile Diameter (mm)**	1.65	1.88
3	**Ramp Angle (°)**	57	64
4	**Friction Coefficient**	0.08	.117

which leads to higher bending moments and more deformation is required to fit through the gear. Although the stresses may rise on the new ring, there is no plastic deformation even on the largest ring tested in the DOE. There were always small regions where the yielding stress would be reached, this may be explained because sharp contacts increase the stresses considerably as explained earlier by [13]. The only plastic strain which was identified was on the contact to the gear where high shear loads take place. The marks are on the same places as in the samples obtained when testing the oval rings in the UTM.

4.5.3 Factors of Interest

In order to obtain a response surface which maps the output from the factors, a Central Composite Design (CCD) was used. Unlike one variable at a time experiments, CCD identifies the quadratic interactions of the factors. The Circumscribed Central Composite Design (CCCD) was chosen as it places the star points outside of the range of possible values. For this study, it is unknown where the optimal values may be and therefore, using an Inscribed or Face CCD would limit the study range. More about CCCD and other response surface tools is explained in [18]. The factorial design can be seen in Table 4.4.

Values are taken as cube points because it is unknown if they are the optimal ones and the range of the study will be expanded by the star points. The alpha value used was 2 and no experiments were repeated since the computational model shows zero variation in its results. The output was the maximum pull out force registered by the FEM model. The resultant experiment contains 25 samples and the full table is attached in the appendix Table A.1. By using Minitab, the DOE was easily created and the following results were obtained.

The Pareto chart from Figure 4.55 shows that all 4 factors have a big impact on the pull out forces but the OD and the Ramp Angle of the gear have the highest. It was observed that the OD had the greatest effect on the pull out force, this was because while it was deformed, it had contact with a greater number of splines. Having understood this, more contact with the splines can be achieved by changing the design slightly and making the ring more round. As explained before, the highest stresses are bending stresses and they depend on the initial diameter. Besides from increasing the stress on the ring, the OD cannot be too large because then the normal axis of the ring would stick out from the shaft. This could potentially have a contact with a flat face like the opening on the gear and get stuck. For these

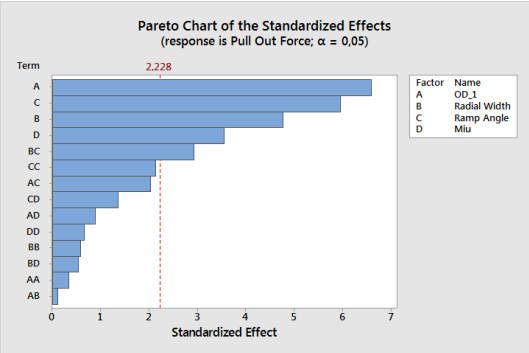

Figure 4.55: Pareto chart for the weight of the factors

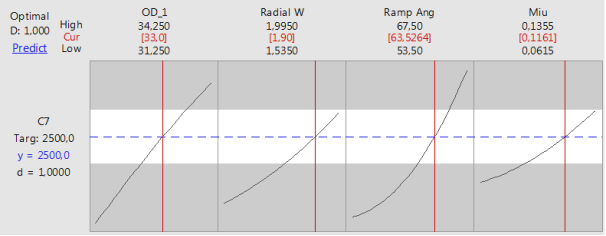

Figure 4.56: Main effects plot with an optimized value of 2,500 N

reasons, the OD is suggested to be smaller than 33 mm.

The friction does not have much impact on the pull out forces possibly due to the small contact area compared to the current ring. The ramp angle shows a misleading effect when decreasing it as the pull out forces start to rise. This however, is the same effect as in the experimental studies in the UTM. While it has been proved that a smaller ramp angle yields lower axial forces just by comparing to the assembly, where the ramp angle is of only 25° and the forces are fairly low compared to disassembly.

Figure 4.56 shows the optimal values to obtain 2,500 N in pull out force. Disassembly forces for the newly designed ring are much smaller than the current snap ring and this is why the optimal shows a higher ramp angle and a larger cross section. The OD was set as 33 mm and can acquaint for usual tolerances of around ± 0.25 mm. The radial width has lower manufacturing tolerances and was set smaller than the limit where it would get stuck between the gear and the shaft. The model then can be used to consider the tolerances for the ramp angle and where the friction coefficient may be. The formula obtained by the response surface is the following.

$$\begin{aligned} PullOutForce = 99438 + 367OD_1 - 25354RadialWidth - 2856RampAngle - \\ 182578Miu - 32,1OD_1 * OD_1 + 2346RadialWidth * RadialWidth + \\ 9,33RampAngle * RampAngle + 103349Miu * Miu - 63OD_1 * RadialWidth + \\ 34,9OD_1 * RampAngle + 2875OD_1 * Miu + 327RadialWidth * RampAngle + \\ 11430RadialWidth * Miu + 946RampAngle * Miu \end{aligned} \tag{4.12}$$

The relation with the ramp angle and the friction coefficient in Figure 4.57 is interesting as it shows how the gear would affect the pull out forces. It can be seen that the pull out forces escalate with a high ramp angle and a rough surface. This may be because the friction forces directly oppose the sliding of the ring and the normal forces opposing the axial force increases with a bigger ramp angle.

Lastly, the contour plot in Figure 4.58 offers a very visual way of identifying the disassembly force by modifying the most important factors. The friction was set to a high value to make sure forces won't be higher than expected. The profile diameter was fixed at a medium value and the manufacturing variations won't make a large difference. Based on this plot, the ring can be designed and also consider the worst case tolerances for the OD and the ramp angle on the gear.

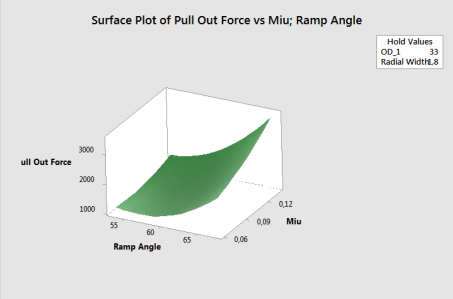

Figure 4.57: Interaction between ramp angle and friction coefficient

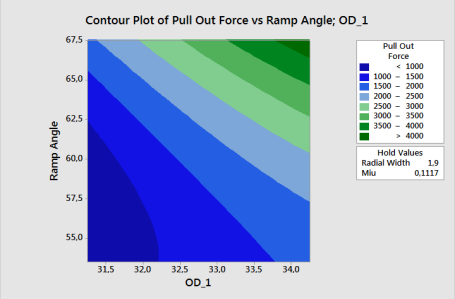

Figure 4.58: Resulting disassembly forces affected by the two main factors

4.5.3.1 Assembly forces

While pull out forces are the greatest challenge for mechanics disassembling the car, the assembly forces cannot be ignored as these could cause great impact in the assembly line, slowing the takt. The same study was performed as in the disassembly forces with the difference that all gears have the same ramp angle of 25°. Values from the same tests were used as the model solved the differential equations both for pushing in and pulling out the shaft. The factors were the same but the ramp angle was eliminated as a factor. The resultant experiment consisted of 15 tests which correlated to 15 out of the 25 experiments from the previous DOE.

Since the ramp angle investigated in the previous DOE only affects step 2 of the model, the results from step 1 of all 25 models were compared. Experiments where for example, an OD of 32 mm, friction coefficient of 0.117 and profile diameter of 1.65 mm should yield the same assembly force in the model with the ramp angle of 57° and 64° from the previous DOE. Since they both had the same assembly ramp angle and this was the initial step. The only difference would be how the mesh was generated on the gear even when the mesh size was the same. Results could vary up to 6% in the assembly force. For this reason, smaller meshes were tried but would mostly end up not converging and with very large processing times.

It was noted that with a finer mesh, axial forces went slightly lower than with the mesh used in this study and in order to get results closer to reality, the mesh would need to be fairly small to represent the round profile accurately. Due to the model being hard to converge and the time limit, a mesh convergence test was not properly performed and it is recommended to perform one for any model of this kind in future

occasions.

The Pareto chart shows that the most important factors are the OD and the radial width, where the friction coefficient shows a smaller impact on the assembly force. This can be compared to the interaction surface plot from Figure 4.57 where the interaction of the ramp angle and the friction, has a big impact on the axial force. Since in this DOE the ramp angle was only 25°. the normal force becomes almost entirely axial and therefore friction may not have much impact on the axial force.

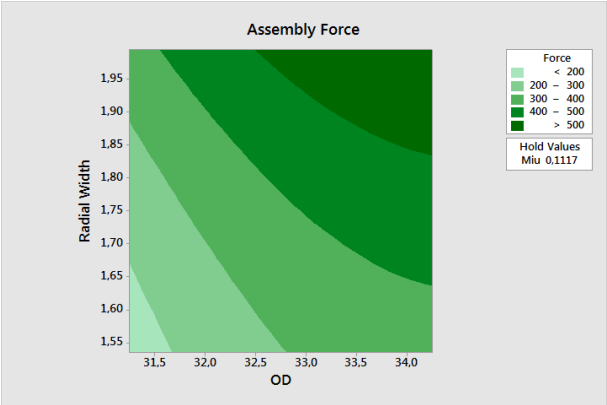

Figure 4.59: Resulting assembly forces affected by the two main factors

From Figure 4.59, to obtain an assembly force of 350 N, it is desired to be in the middle region of the plot, meaning that either the profile diameter has to be close to 2 mm or the OD has to be close to 33 mm. Comparing back to the contour plot from the previous DOE, the optimal values of OD 33 mm and profile diameter close to 1,9 mm would result in assembly forces of between 400 and 500 N. To prevent this, a smaller ramp angle at the entrance of the gear can be used. More tests should be considered however.

Several ramp angles where tested under the same friction coefficients and same ring geometries. When comparing the assembly and disassembly results, it can be noticed that there is a close relation between the quotient of two forces and the quotient of the tangent between both ramp angles as seen in Figure 4.60. This means that the quotient of the tangent of two ramp angles can be used to get an estimate between change in axial force required to dismount a shaft with a different ramp angle. This was more accurate in the oval ring as the friction forces were smaller than in the current ring. At a higher ramp angle, the relation starts to diverge due to the interaction identified in Figure 4.57. The (4.13) shows the relation between the ramp angles and the axial forces.

$$\frac{\tan(a)}{\tan(b)} \sim \frac{F_a}{F_b} \tag{4.13}$$

Where a is a new angle, b is 25° and F is the axial force obtained with different ramp angles in the DOE. The equation has a limited range of values and should be

investigated further but it correlates with the analytical study of the axial forces where the friction was assumed as zero.

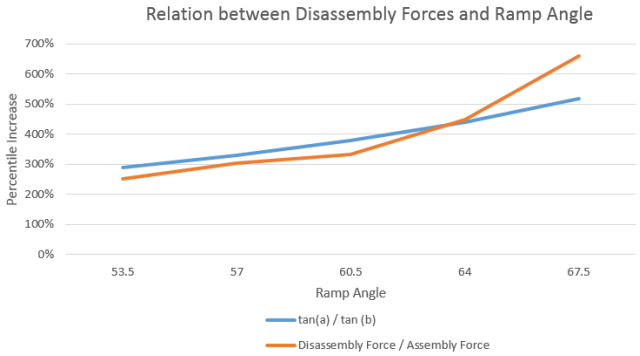

Figure 4.60: Relation between ramp angles and axial forces

4.5.4 Additional Tests

Some additional tests performed to increase the understanding of the interface are reported in this subsection. Some of the assumptions made by the DOE are also tested here.

4.5.4.1 Increasing Axial Forces

In order to understand how the axial forces are changed by increasing the contact between the ring and the gear, a new design was tested. This design is no longer based on an oval geometry but instead is aimed to increase the contact with the splines on the gear by enlarging the ring in the blue region as shown in Figure 4.61.

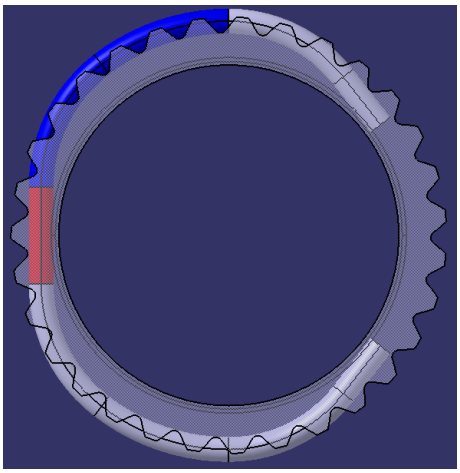

Figure 4.61: Modified oval ring

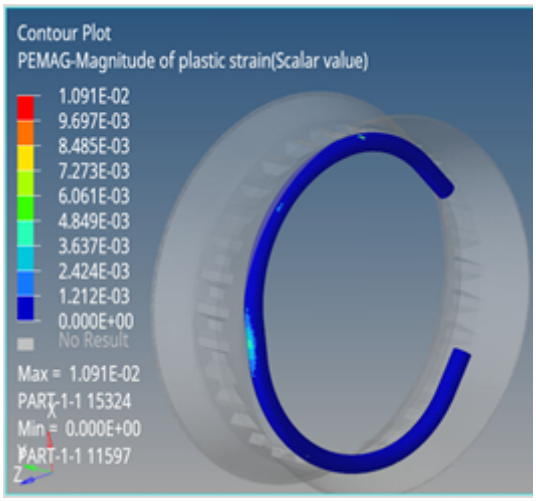

Figure 4.62: Plastic deformation in the ring after disassembly

New design managed to decrease the OD to 32.5 mm and increased the pull out force to 2,100 N but the ring has too large stresses, just above the yielding point. The assembly force was kept lower than the limit. By modifying the blue arc and making it even larger, the forces rose significantly, one more test was performed and a pull out force of 3,100 N was obtained. The red section acts as a stress concentration and has the highest stresses where the ring suffers some permanent deformation as shown below in Figure 4.62. For this reason, this design is not recommended but it was helpful to understand how to increase the pull out forces and decrease the max OD in order to keep the ring's normal axis inside the groove.

4.5.4.2 Missing Splines

The assumption that the missing splines did not affect the disassembly was tested. A gear with the two missing splines was implemented in the model and a few simulations were done. All of them would fail due to the contact illustrated in Figure 4.63. Although this contact also occurs in gears without missing splines, the other open ends hangs loose and the contact is rotated as seen in Figure 4.64. Simulations were never fully converged for this model due to this contact issue and would suggest that a locking mechanism could occur easier due to the missing splines. As mentioned below, if its not possible to increase the air gap to let air to come out during assembly nor to remove the cap which keeps the gear sealed, the oval ring should still prevent this issue as no open ends will come close to the gap created by the missing splines.

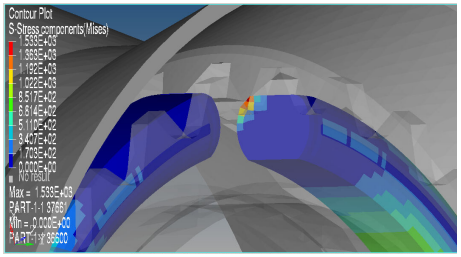

Figure 4.63: Contact in model with missing splines

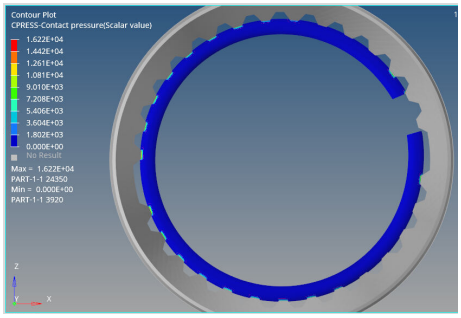

Figure 4.64: Effect on contact forces when having missing splines

4.5.4.3 Using Flexible Bodies

Besides from the initial simulation where flexible bodies were used, some more attempts were done at the end of this study to correlate how the simulation is affected by the rigid body assumption. A new model was developed based on the one with the current ring as there was more data to compare with. Geometries were modified as previous simulations used very thin bodies for the shaft and gears. The new model took almost 48 hours to compute and showed much higher forces than the base model. It is important to note that this model was very delicate to friction

coefficient changes. The force when sliding through the gear was also much higher than measured in reality and no more attempts were done to obtain a good correlation due to the time constraint.

Results from the simulation with flexible bodies show very small stresses on the gear even with high disassembly forces but no locking mechanism. Previous experimental tests have shown small marks on the gear splines which may have been created by the open ends of the ring or deformed shaft splines. The simulation didn't show any permanent deformation on the shaft and the stress concentration on the root of the splines may be cause due to poor meshing as seen in Figure 4.65. This means that under normal sliding conditions for a ring, the shaft and gear should remain intact.

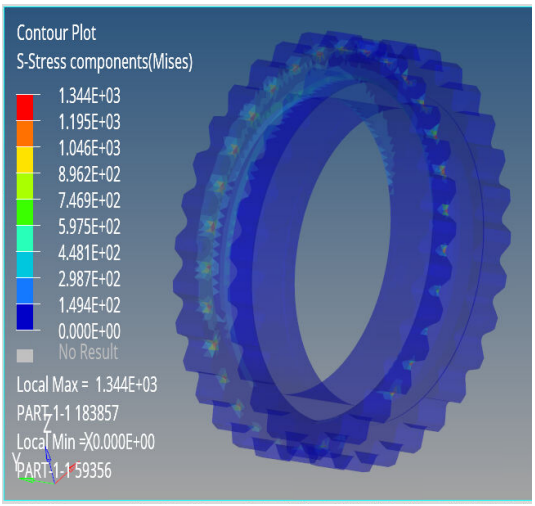

Figure 4.65: Highest stresses on the shaft during disassembly

4.5.4.4 Assembly Stresses on the Snap Ring

To calculate the stresses on the ring when assembling it radially into the shaft, a new model was developed. The model fixed the shaft as a rigid body and half of the ring would be displaced vertically from the shaft while having contact with the open end and the shaft. This would simulate the bending stresses on the ring and identify if there was any plastic deformation after assembling the ring into the shaft. The maximum stresses can be seen in Figure 4.66.

Results show that the extrados and intrados of the ring reach their yield strength value and will have a permanent deformation as seen in Figure 4.67. This deformation will permanently increase the OD of the ring by about 1 mm and may be considered as acceptable. However it also means that the ring will hang slightly on the shaft and that pull out forces could be higher than this study anticipated in the previous experiments. While more studies could be done to prevent this plastic deformation, creating a fillet on the intrados of the ring and increasing the gap

on the ring, it is unsure whether this permanent deformation is so critical. Under the assumption that the ring is circular, (4.6) can be used to estimate the bending stresses when assembling the ring using a different gap. It is also unknown whether it is possible for suppliers to bend the ring directly into the shaft, this would save the assembly process and the stresses from the radial assembly would be prevented.

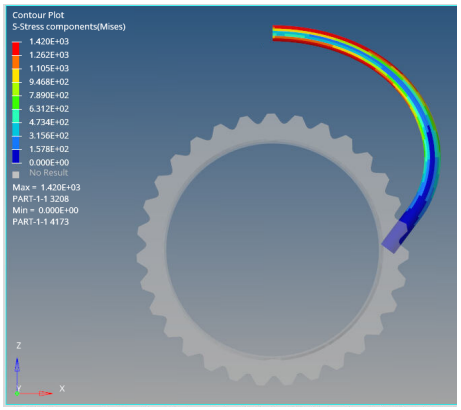

Figure 4.66: Maximum stresses on half a ring when assembling it into the shaft

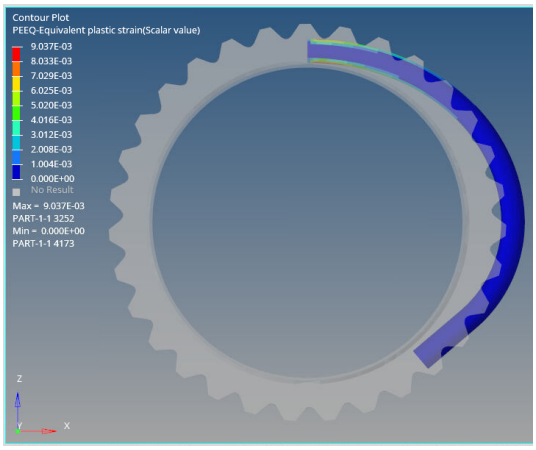

Figure 4.67: Plastic strains on the ring after assembly

4.5.4.5 Groove Depth

The groove depth has to be large enough to keep clear the radial thickness of the ring when being deformed and sliding through the gears minimum diameter. As seen on the previous simulation, having sections of the ring straight as the red surface in Figure 4.61 acts as a stress concentration and will most likely lead to a permanent deformation. For this reason it is recommended to keep the shape of the ring as an ellipse. The relation between the major and minor axis can be modified to have more contact with the gear splines (to increase the pull out force required) and to keep contact with the bottom of the shaft's groove.

It is important to keep the open ends of the ring within the groove and the gear minor diameter, this region will be denominated as the safe region and is represented by the green area in Figure 4.69. If the open ends exit this region during deformation, a locking mechanism could occur. The open ends should always be tangent to the bottom of the groove and design has to acquaint for manufacturing tolerances. The cut on the open end can even have a chamfer or a fillet as seen in Figure 4.68, to help the ring slide during assembly or in case the ring tries to dig into the shaft. The fillet on the extrados can't be too large as some surface is needed to easily push the ring out of the shaft when dismounting it. This could also decrease the stresses when assembling the ring into the shaft.

Adjusting the relation between the major and minor axis will affect the groove depth. Increasing the groove depth helps to keep the open ends of the rings within the safe

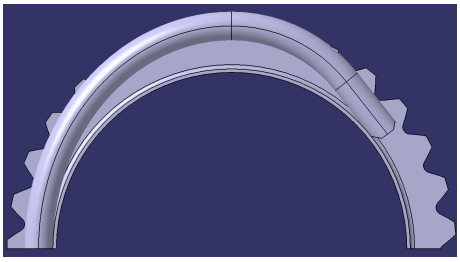

Figure 4.68: Resulting assembly forces affected by the two main factors

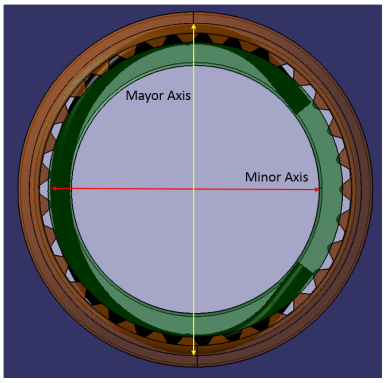

Figure 4.69: Plastic deformation in the ring after disassembly

region during deformation but will decrease the contact with the gear splines, making it possibly too easy to disassemble. It is not recommended that the neutral axis of the ring goes beyond the splines of the gear as this could have a contact with a flat surface getting locked. Additionally, increases the bending stresses on the ring. As mentioned before if the shaft's groove is increased, it has to be analyzed further, therefore it is easier to adjust the ring's minor and major axles to the allowed groove depth.

4.5.4.6 Modified Material

Finally, some simulations were performed in order to help design a ring for a shaft with a smaller spline modulus. There had been some issues before where the ring would reach very high assembly forces and equally large disassembly forces. Something strange under the assumption that the exit ramp angle was larger than the entry ramp angle. The spline modulus used was of only 0.78 and the profile of the ring was 2 mm. There was very limited data available to make this simulation so different materials were tested trying to understand what the issue was. Figure 4.70 shows the disassembly forces using materials with different Young's modulus.

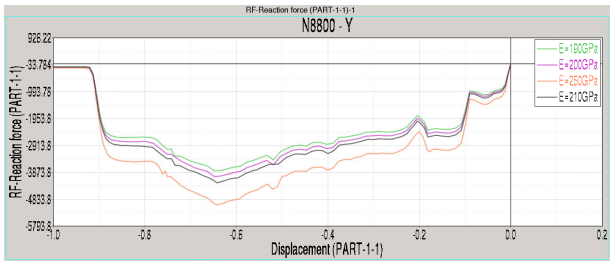

Figure 4.70: Effect on the Young's modulus of the material on disassembly forces

Later on, it was found that the ring was slightly over dimensioned in OD and profile diameter and had a low yield strength. This caused large bending stresses during

assembly and thus plastically deforming. During disassembly, the ring had already been deformed in such a way that the contact between the ring and the gear was lesser and thus even with a higher ramp angle, the force was almost the same as the assembly force.

The learning outcome from this test is that the rings material should be strong enough to withstand the bending stresses. However, any steel should work well as using a stiffer material, will also make the system harder to dismount and most likely increase the cost as well. When having a lower spline modulus, the ring can also be smaller as less contact is needed to keep the interface locked.

5
Recommendations

In this section, the methods will be discussed and a summary of the recommendations for the interface design is presented. Recommendations for future research are also found here.

5.1 Methods

While the mathematical model of the split rings works quite well for thin rings under small deformations, it is unknown how reliable it is for the deformations that the analyzed snap ring suffers. Additionally, the splines also play a big role which is not considered in the model. Lastly, the mathematical model works under the assumption that the load is distributed along the extrados, just like it was performed in the ANSYS model, however, this is not accurate in the reality. For this reason, the radial forces were unable to be estimated numerically. Focusing more in a governing equation for all rings would have taken too long time. Furthermore, focusing only on this wouldn't have solved the problem of the shafts getting stuck.

Regarding the experimental testing with the UTM, it could be questioned whether the method for centering the plots for each individual data set is right but was the best option found with the available resources. The proposed oval ring design would need to be tested a significant number of times without getting stuck in order to statistically prove that the design is reliable. However, since all samples were modified by hand, this resulted in high geometrical variations and affected the axial forces obtained when testing the ring in the UTM. The direction of the assembly was also questioned. It can be argued that the ring does not hang loose when assembled as it sits slightly compressed on the gears bore and thus, the direction should not affect the axial forces obtained. Fixing the shaft instead of the gear was also proved not to cause any variations in the FEM model.

The factors identified as responsible for the shaft getting stuck are the following and should be avoided with any ring design.

- Having a too small gap may cause open ends to touch.
- Hitting with a hammer without successfully removing the shaft may damage the ring.
- Getting the open ends stuck between the splines was a recurring problem and

is because the open ends close into a spline.

- In rings with bent tips:
  1. Having bends with a sharp angle may end up sticking out of the safe zone and be sheared as happened with ring #2.
  2. Open ends not being tangent to the shafts groove bottom may cause the open ends to dig into the shaft instead of sliding and thus, blocking the deformation at A.
  3. Have an open end stick out of the safe zone during deformation.
- Having a damaged shaft which doesn't have a perpendicular contact with the ring.
- Having a very high ramp angle and a very poor surface roughness. Refer to 2.7 for the minimum ramp angle allowed to a certain friction coefficient.

The dynamic testing was performed under very limited time and results can't be very accurate. The only purpose of performing this study was to relate the axial forces obtained from the UTM to the force which an operator would have to apply on the tool to dismount the shaft. Results showed that removing a ring when it is not stuck wouldn't pose a big challenge for a mechanic. Both the lever and the wedge tools worked fine and a further discussion should be done to decide which to choose as the official tool for the proposed interface. For the current interface, the wedge seemed to work better as the space needed is smaller. Reducing the angle of the wedge worked well but could mean that the same tool for shafts from different cars can't be used as explained in 4.2.2.1. It is recommended however, not to apply brute force when hitting the wedge with a hammer as it could create dents on the ring and make it harder to dismount. Instructions for disassembly should then mention that if the shaft is not dismounted after some gentle strokes, the shaft should be rotated to try to reset the rings angular position. After doing so, the wedge tool can be used again but never trying out to hit the wedge as hard as possible with the hammer.

Regarding the FEM model, many things can be discussed about it. First, the assumption of having a rigid model may give a larger variation than expected as it wont allow the hertzian contact on the shaft and the gear. Secondly, since the surface of the bodies is so important, the mesh would be questioned. Even after setting a fairly small element size of 0.25 -0.4 mm, the contact established between the bodies is not perfect. A mesh convergence study should also be performed as even after using the same element length on the rings results where up to 6% different even when the same test was performed.

Although the friction coefficient was estimated, it was done under the assumption that the force was applied evenly on the extrados of the ring. In reality, the forces would be higher, making the friction coefficient even smaller. It was decided to use the obtained coefficient nevertheless to obtain results which would occur under worst circumstances. Some of the curves between experimental testing and simulations are very similar, this could mean that the coefficients are actually close to reality. It was also shown in Figure 4.51 that the friction coefficient acts as a scaling factor for

the axial force. However, since there was so much variability in the UTM testing, there was not a single value to approximate to.

Although the model showed a good correlation to some of the tests, further correlation can be achieved. The results from the DOE will not be perfectly accurate but can be used to understand how the parameters affect the result and around which values should the axial forces be expected.

What could be tested as a parameter in a new DOE is the interference volume, or the volume that the ring has to be deformed in order to fit the gear. Although the contact would still be very limited, understanding the relation between deformation, friction and disassembly force could further help the optimal design of a snap ring.

5.2 Final Recommendations

In the end, the factor which caused a bigger variation of the assembly and disassembly forces was the geometry of the ring due to the amount of interference and deformation needed to enter the gear. Some extra recommendations are as follows:

- Change the ring to a radial ring with an oval shape to reduce the interference.
- Change the cross section to round.
- Keep the open ends inside the safe area and consider the manufacturing tolerances. Also consider 4.5, the extrados of the ring must be smaller than the minor diameter of the gear.
- Keep the surface roughness as low as possible to allow the ring to slide without any impediments.

Regarding the rings geometry, the proposed oval design does not have any bent tips as they act as a stress concentration location and are prompt of getting stuck during deformation. There is a constant trade off when deciding the final dimensions of the ring and Figure 4.58 can be used to decide them as well as seeing how the possible tolerances would affect. If the ring is designed for 2,500 N, the assembly force will most likely increase and for that reason, the assembly ramp angle would need to be slightly decreased. 4.13 Can be used for this purpose and it should be remembered that this is an approximation and the valid values for the equation is limited.

The cross section is proposed as round as the OD can be increased more than the current profile before it has a tangential contact with a vertical face in any other body or an unusually deep bore on the gear which would cause a locking mechanism. This issue has been reported before in other projects and hence why is taken into consideration. The second consideration is that reducing the cross section radii is favorable to transform the axial forces into radial forces instead. At the same time, the round profile is easier to shear in case it gets stuck for any reason.

After understanding what causes the variations in the disassembly forces the dimensions for the investigated interface is propposed. Future research can be done in

order to make the dimensions scalable for other interfaces. Although it was found that the maximum OD should be around the same as the gear mayor diameter and the profile diameter not more than twice that of the modulus. Some more research should be done to validate that this is in fact, scalable. Parameters can be modified to have some trade offs between axial forces and stresses.

Having a slightly bowed ring seems to be easier to disassemble in reality and it also helps to keep the ring in place and not hanging loose. More studies on this should be done as they only .

The material is recommended to be kept as a steel as the bending stresses are quite high and the ring needs a good hardening process to be able to withstand these loads without yielding. It is also recommended because it will be harder to create dents in it which can lock it in place.

Regarding the surface roughness on the gear, it was shown that it is not the main cause of the problem since even ground surfaces with a lower ramp angle got a ring stuck in place. Additionally, some bench marked gears had a higher surface roughness. On the other hand, from the DOE and the Snap theory it was learned that there is an interaction between the ramp angle and the friction coefficient so keeping it as smooth as possible could help keep the forces low. From the theory, many papers also mention that the surface roughness is correlated to the friction coefficient and from the FEM experiments performed in this study, axial forces were also proportional to it. It is also important to remember that the friction coefficient is something engineers have to live with. What can be understood from this study is that the surface roughness doesn't have to be perfectly smooth but shouldn't have big burrs which may act as a physical stop for the ring to slide.

Simulations show that the proposed ring will most likely have a permanent deformation after it is assembled into the shaft, it would be questioned whether this is acceptable or not. There are several ways of fixing this issue by increasing the gap slightly would be the quickest option. The open ends should always be tangent from the groove bottom to prevent them from getting stuck when compressing and tolerances for the gap should be considered. A further analysis of (4.7) can help estimate an optimal gap according to the yield strength of the material assuming that the ring is round in geometry. If taking the d as the distance the open tips have to deform in order to slide through the shaft when assembling, the force can be applied in the opposite direction to open the ring. The bending stresses can then be calculated and the gap designed accordingly.

A summary of the recommendations found in this study can be found in Table 5.1:

As mentioned before, a small fillet between the intrados and the open ends could help the ring have a sliding motion to the shaft in case the open ends are not tangent to the groove bottom for any reason. This can be easily fixed by using a different tool when cutting the ring after coiling it. The fillet should not be so large so that a

Table 5.1: Design recommendations for the most influential parameters analyzed in this study

Parameter	**Recommendation**
Material	Steel
Heat Treatment	High Yield Strength
Assembly Ramp Angle	25°
Disassembly Ramp Angle	58°-62°
Bore Diameter	≈ Gear mayor diameter
Groove Diameter	<Gear Minor diameter + 2 * Profile diameter + SF
OD	Not much larger than the gear mayor diameter in worst possible tolerance
Gap	d = R_{Groove} - $\frac{Gap}{2}$ (4.6) Depends on the yielding strength of the material
Profile Diameter	≈ 2 * Spline modulus
Surface Roughness	R_z <12.5; as smooth as possible
Wedge Angle on tool	As low as possible considering available space and other shaft model

good contact surface can be obtained when removing the ring from the shaft. The extrados can also have a small fillet to prevent it from closing into a spline from the gear. These are preventive measures and should not occur in the proposed design if the tolerances are properly specified.

6
Conclusion

Although a very small component, a snap ring and the interface with the drive shaft and a gear is often disregarded and not designed properly, resulting in high costs when dismounting it and slowing down the development process as many iterations need to be tested by trial and error. The same interface is used by several car manufacturers due to the simple assembly and disassembly process. This thesis investigated the reason for drive shafts to have a variation in disassembly forces and proposes an optimized interface. High disassembly forces causes mechanics to have very poor ergonomics when dismounting the drive shaft and it is important to keep low during assembly to keep up with the takt in the assembly. The study thereby tested many parameters to create an extensive understanding of how the interface affects the axial forces needed to dismount the system.

A mathematical model was developed in section 2.4 in order to estimate the axial forces required to assemble or disassemble the interface. The model was not successful as it is more complicated in reality and it would take too long to develop an accurate mathematical model. Additionally, the mathematical model would not be able to identify possible locking mechanisms. For this reasons the mathematical model was abandoned and moved on to physical experiments.

Some parameters of the interface were tested in the workshop and later on in a UTM to obtain accurate data, this is reported in section 4.3.1. The tests showed a very high variation in measured axial forces. Several issues were found on the interface and reported, this helped design a new ring which would prevent the system to get locked. Results from different disassembly tools also show that both a wedge and a lever tool worked well with a properly designed ring which would not get stuck.

The proposed new rings showed even too low disassembly forces and a DOE was needed to optimize the factors to achieve a desired disassembly force which is within Volvo's internal specifications. In order to perform a DOE with significant results, the variability from the tests would need to be reduced significantly. Using CAE, a computational model was developed saving long lead times and costs in manufacturing of more samples to further test the remaining parameters with. The model would show a nominal result and was used for the DOE.

A FEM model which simulated the assembly and disassembly of the system in a non linear, static, implicit simulation using ANSA was built and reported in section 4.4. The model was very sensible for small changes in geometry, mesh and friction

coefficient due to the contact between the bodies. Correlation to some extent was obtained based on previous data gathered by the physical experiments. In order to get a better correlation, the model can still be improved based on the recommendations from the previous section.

Based on the computational model, a CCCD was performed in section 4.5, taking the resultant axial forces as the output and the OD, friction coefficient, profile diameter and ramp angle as factors. Data was processed using Minitab in order to obtain the response surface which creates a regression from the data to approximate output values. The result shows graphically the expected assembly and disassembly forces based on changes in the four factors shown in Figures 4.58 and 4.59.

Results from this study can be used as a guideline in order to design snap rings in the future and gives an understanding of how the parameters in the interface affect the assembly and disassembly forces, summarized in section 5.2. Additionally, many issues which cause the interface to get stuck are listed in 5.1. The proposed design considers all the identified locking mechanisms and offers an optimized interface. A correct interface will keep the assembly forces low so takt is not affected during production. The ergonomics of the mechanics will be improved during the disassembly and there will not be a need for special tools to remove the shafts.

Bibliography

[1] V. C. Corporation, "Anual report 2019", Volvo Car Corporation, VAK building, Assar Gabrielssons väg Göteborg, Sweden, Tech. Rep., Jan. 2020, https://investors.volvocars.com/ /media/Files/V/Volvo-Cars-IR/results-center/2019/volvocargroupannualreport2019.pdf.

[2] A. Gungor and S. Gupta, "Disassembly sequence planning for products with defective parts in product recovery", *Computer & Industrial Engineering*, vol. 35, pp. 161–164, Oct. 1998. DOI: 10.1016/S0360-8352(98)00047-3.

[3] P. Spring, *Retaining rings technical manual*, Online Handbook, Manufacturers of Engineered metal products, 1625 Commerce Road, Holland.

[4] Rotorclip, *Ultimate retaining ring guide*, Online Handbook, Rotor Clip Company, Davidson Avenue, Somerset, NJ, USA, 2010.

[5] R. Hubener, *Seeger rings a designer's handbook*, Online Handbook, Seeger Orbis GmbH, D-6240 Königstein Taunus - West Germany.

[6] J. R. Barber, *Contact Mechanics*, ser. 6557. Ann Arbor, MI, USA: Springer, 2018, Page 267, ISBN: 978-3-319-70939-0.

[7] E. Dragoni and A. Strozzi, "Analysis of a split ring inserted onto a circular housing", *Strain analysis*, vol. 21, no. 2, pp. 59–70, Apr. 1986, Universita di Bologna, Italy. DOI: https://doi.org/10.1243/03093247V212059.

[8] A. Strozzi, E. Bertocchi, and A. Baldini, "Contact stresses within a split ring inserted into a circular housing", *The Journal of Strain Analysis for Engineering Design*, pp. 672–688, Nov. 2009, https://www.researchgate.net/publication/245394737. DOI: DOI:10.1243/03093247JSA542.

[9] J. R. Barber, *Designing Plastic Parts for Assembly*, 8th ed. P.O. Box 7747 Bloomfield Hills MI 48302-7747: Hanser, 2017, Page 261, ISBN: 978-1-56990-668-2.

[10] Mitutoyo, *Quick guide to surface roughness measurement*, Online Handbook, https://www.mitutoyo.com/wp-content/uploads/2012/11/1984_Surf_Roughness_PG.pdf, Aurora, Illinois, USA, Dec. 2016.

[11] B. Ivkovic, M. Djukdjanovic, and D. Stamenkovic, "The influence of the contact surface roughness on the static friction coefficient", *Tribology in the Industry*, vol. 22, pp. 41–44, 2000, UDK 62r.9.0r5.0.

[12] P. L. Menezes, Kishore, and S. V. Kailas, "Influence of roughness parameters on coefficient of friction under lubricated conditions", *Sadhana*, vol. 33, pp. 181–190, 2008, https://www.ias.ac.in/article/fulltext/sadh/033/03/0181-0190.

[13] A. Strozzi, A. Baldini, M. Giacopini, E. Bertocchi, and L. Bertocchi, "Normalization of the stress concentrations at the rounded edges of a shaft–hub inter-

ference fit", *The Journal of Strain Analysis for Engineering Design*, vol. 46, pp. 478–491, Dec. 2010, University of Modena and Reggio Emilia, Modena, Italy. DOI: DOI:10.1177/0309324711403845.

[14] D. M. Hamby, "A review of techniques for parameter sensitivity analysis of environmental models", *Environmental Monitoring and Assessment*, pp. 135–154, 1994, http://citeseerx.ist.psu.edu/viewdoc/download?doi=10.1.1.224.7813&rep=rep1& type=pdf.

[15] M. F. del Olmo Heres and A. F. Schmidt, "Clips and brackets. assembly & disassembly force", ISSN 1652-8557, Master's thesis, Chalmers University of Technology, Department of Applied Mechanics Division of Dynamics Chalmers University of Technology SE-412 96 Göteborg Sweden, 2017.

[16] E. Cronqvist and L. Sundler, "Parametrical study of a splined shaft", Examensarbete No. 136/2015, Master's thesis, Chalmers University of Technology, Göteborg, Sweden, 2015.

[17] M. Mägi, K. Melkersson, and M. Evertsson, *Maskinelement*, 8th ed. Studentlitteratur, 2017, ISBN: 978-91-44-10905-3.

[18] S. S. Ranade and P. Thiagarajan, "Selection of a design for response surface", *IOP Conference Series: Materials Science and Engineering*, vol. 14, no. 263, pp. 201–213, Dec. 2017. DOI: doi:10.1088/1757-899X/263/2/022043.

A

Appendix 1

Some of the results not reported previously can be found here. The rest of the documents can be found in the folder delivered to the supervisor.

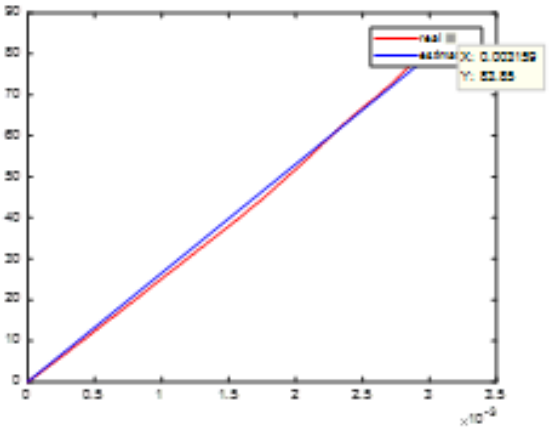

Figure A.1: Correlation between theoretical and experimental vertical compression of the current ring

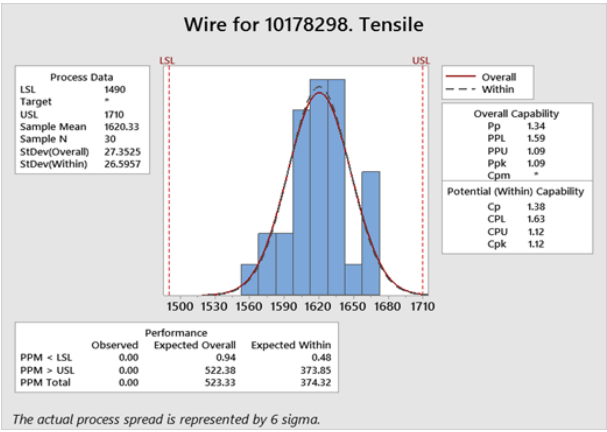

Figure A.2: Mechanical Properties of the hardened steel for the current ring

Table A.1: Design table with results used in both DOE

Run Order	OD (mm)	Radial Width (mm)	Ramp Angle	Friction Coefficient	Pull Out Force (N)	Push In Force (N)
1	32,00	1,650	57,0	0,0800	634,60	253
2	33,50	1,650	57,0	0,0800	1354,20	378
3	32,00	1,880	57,0	0,0800	995,98	370
4	33,50	1,880	57,0	0,0800	1407,82	474
5	32,00	1,650	64,0	0,0800	856,90	250.9
6	33,50	1,650	64,0	0,0800	1543,30	360
7	32,00	1,880	64,0	0,0800	1360,18	361
8	33,50	1,880	64,0	0,0800	2362,06	447.1
9	32,00	1,650	57,0	0,1170	781,33	287.1
10	33,50	1,650	57,0	0,1170	1643,19	440.3
11	32,00	1,880	57,0	0,1170	1237,57	420.8
12	33,50	1,880	57,0	0,1170	1650,31	511.3
13	32,00	1,650	64,0	0,1170	1132,61	277.7
14	33,50	1,650	64,0	0,1170	2047,31	434
15	32,00	1,880	64,0	0,1170	1787,05	411.6
16	33,50	1,880	64,0	0,1170	3055,63	513.1
17	31,25	1,765	60,5	0,0985	251,45	194.2
18	34,25	1,765	60,5	0,0985	2044,32	462.8
19	32,75	1,535	60,5	0,0985	1091,53	311
20	32,75	1,995	60,5	0,0985	1596,80	460.7
21	32,75	1,765	53,5	0,0985	970,87	384
22	32,75	1,765	67,5	0,0985	2383,76	360.8
23	32,75	1,765	60,5	0,0615	1028,78	337
24	32,75	1,765	60,5	0,1355	1694,30	411.7
25	32,75	1,765	60,5	0,0985	1291,99	372.8

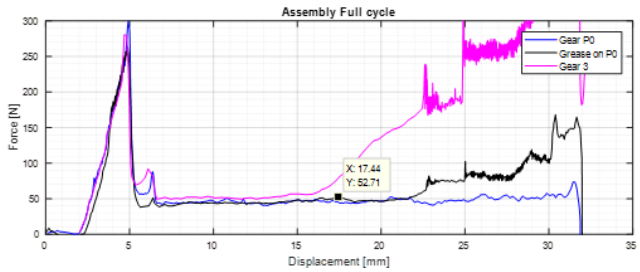

Figure A.3: Full Assembly plot for Current Ring

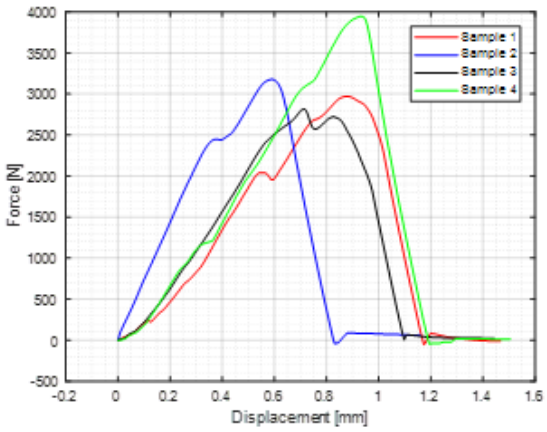

Figure A.4: Disassembly plot for Current ring with grease applied

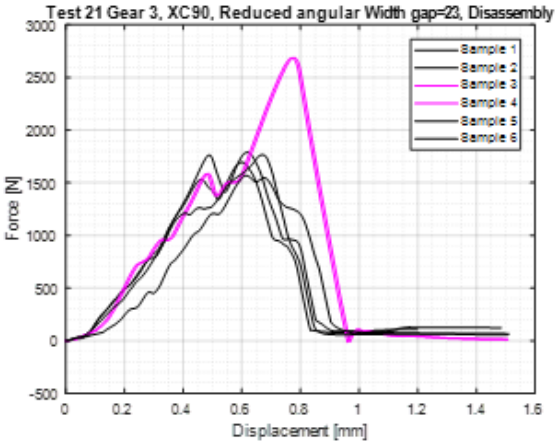

Figure A.5: Disassembly of current ring with different gap distances

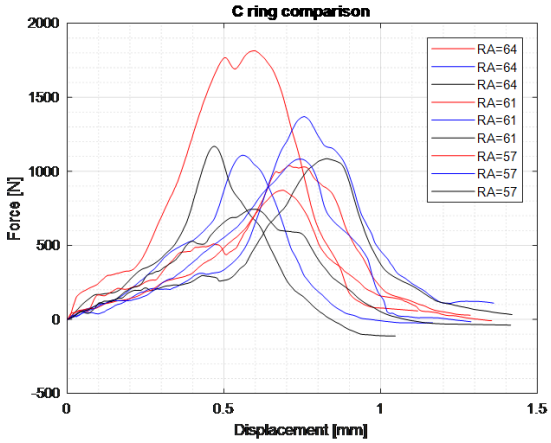

Figure A.6: Disassembly of oval ring with different Ramp Angles

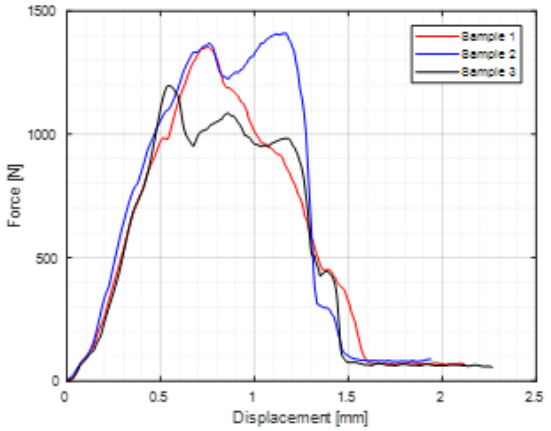

Figure A.7: Disassembly of Benchmarked ring

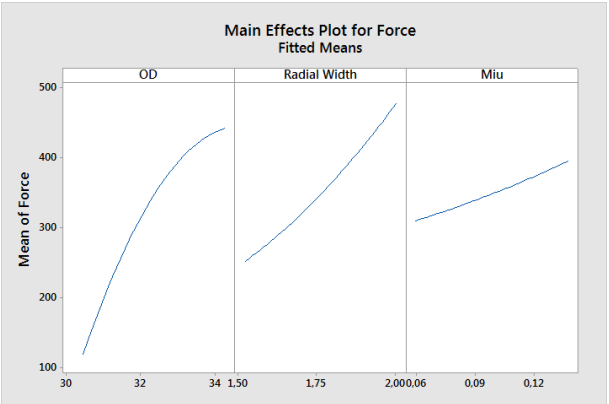

Figure A.8: Main Effect Plot for Diassembly of the oval ring

Figure A.9: Disassembly Tools used by the workshop